

The Importance of the Pre-exponential Factor in Semiclassical Molecular Dynamics

Giovanni Di Liberto and Michele Ceotto

Dipartimento di Chimica, Università degli Studi di Milano, via Golgi 19, 20133 Milano, Italy

Abstract

This paper deals with the critical issue of approximating the pre-exponential factor in semiclassical molecular dynamics. The pre-exponential factor is important because it accounts for the quantum contribution to the semiclassical propagator of the classical Feynman path fluctuations. Pre-exponential factor approximations are necessary when chaotic or complex systems are simulated. We introduced pre-exponential factor approximations based either on analytical considerations or numerical regularization. The approximations are tested for power spectrum calculations of more and more chaotic model systems and on several molecules, for which exact quantum mechanical values are available. The results show that the pre-exponential factor approximations introduced are accurate enough to be safely employed for semiclassical simulations of complex systems.

I. INTRODUCTION

Semiclassical (SC) molecular dynamics is a well established molecular dynamics approach for including all quantum effects starting from classical trajectories.[1–3] Since its introduction,[4] the Semiclassical Initial Value Representation (SC-IVR) formulation of the semiclassical propagator in the coherent state representations[5–7] has become a molecular dynamics tool that embodies accuracy and, at the same time, practicability.[8–28] SC-IVR depends only on local potential and it is very promising for the future, since it has been implemented with “on the fly” direct molecular dynamics approaches,[29–36] allowing for calculations when an analytical fitting of the Potential Energy Surface (PES) is not possible. This aspect is fundamental when pursuing the simulation of complex systems, where the high number of degrees of freedom does not allow for a compact analytical PES formulation.[37–44]

The main stumbling block of the SC-IVR propagator is represented by the pre-exponential factor, which we will describe below. Several approximations has been employed in the past to obviate this limitation. Analytical considerations includes the linearization of the propagator (LSC-IVR) that can be derived also using Wigner’s transform of the quantum operators involved,[19, 45–51], the interaction picture,[40, 52] or the Forward-Backward FB SC-IVR approximation, which is suitable for correlation function calculations.[17, 53–55] Also, the pre-exponential factor can be partially suppressed in a series expansion of the propagator,[15, 56, 57] or totally suppressed in the amplitude-free quasicorrelation function.[58] Numerical considerations lead to the introduction of filtering techniques, such as the one by Filinov[54, 59] or the time averaging one in the instance of spectroscopic calculations.[27, 29–33, 60–64] Considering that during “on the fly” direct dynamics semiclassical simulations, the calculation of the Hessian, necessary at each time-step for the pre-exponential factor calculation, is the computational time bottleneck, a compact finite difference (CFD) numerical approximation for the Hessian has also been implemented.[32, 61]

In this paper, after introducing the origin and the physical importance of the semiclassical pre-exponential factor, we extensively test different approximations to the pre-exponential factor and introduce new ones. The tests are performed on both artificial chaotic systems and real molecules, in order to give a complete overview of the range of applicability of the approximations and provide a reliable tool for complex system simulations. The following

Section presents the motivations of this work and Section III recalls the SC-IVR expression for power spectra calculations. Section IV illustrates the adiabatic approximation of the pre-exponential prefactor, which still implies the numerical integration of the pre-exponential factor components. Section V recalls the “poor person’s” approximation. Section VI formulates the log-derivative representation of the pre-exponential factor which leads to a set of approximations like the harmonic approximation (Section VI A), Johnson’s approximation (Section VI B), one approximation designed by Miller (Section VI C) and, eventually, our new approximations at the end of the same Section. Numerical approximation of the pre-exponential factor are presented in Section VII and numerical tests follow in Section VIII, both for model chaotic systems (Sections VIII A and VIII B) and molecules (Sections VIII C, VIII D, VIII E, VIII F). Section IX concludes the paper.

II. MOTIVATION

In the Feynman’s path integral representation,[65] the quantum propagator going from the starting point \mathbf{q}_0 to the final one \mathbf{q}_t is formulated as a collection of paths

$$\langle \mathbf{q}_t | e^{-i\hat{H}t/\hbar} | \mathbf{q}_0 \rangle = \int_{\mathbf{q}_0}^{\mathbf{q}_t} \mathcal{D}[\mathbf{q}(t)] e^{iS_t[\mathbf{q}_0, \mathbf{q}_t]/\hbar} \quad (1)$$

where $S_t[\mathbf{q}_0, \mathbf{q}_t]$ is the action functional for time t and $\mathcal{D}[\mathbf{q}(t)]$ is the differential over all possible paths (even the infinity length ones!). The main obstacle to the numerical integration of Eq.(1) is given by the oscillatory integrand. A common strategy is to approximate the integral (1) to the contribution that comes from the paths where the phase is stationary, i.e. $\delta S_t[\mathbf{q}(t)] = 0$, provided that starting and ending points are fixed. In this case, Eq.(1) becomes

$$\langle \mathbf{q}_t | e^{-i\hat{H}t/\hbar} | \mathbf{q}_0 \rangle \approx \int_{\mathbf{q}_0}^{\mathbf{q}_t} \mathcal{D}[\mathbf{q}(t)] \exp \left[\frac{i}{\hbar} \left(S_t^{cl}(\mathbf{q}_0, \mathbf{q}_t) + \frac{1}{2} \frac{\delta^2 S_t^{cl}(\mathbf{q}_0, \mathbf{q}_t)}{\delta \mathbf{q}(t)^2} \delta \mathbf{q}(t)^2 \right) \right] \quad (2)$$

where the sum is now restricted to the classical paths from \mathbf{q}_0 to \mathbf{q}_t and $S_t^{cl}(\mathbf{q}_0, \mathbf{q}_t)$ is the action of the classical paths. It is important to stress that Eq.(2) is the embryo of several semiclassical approximations and it accounts not only for the classical paths contributions, but also for the vicinity of each path via second order path fluctuations. The goal of this paper is to determine how important these fluctuations are to “sew quantum mechanical flash onto classical bones”[65, 66] and, thus, for an accurate quantum mechanics description of molecular vibrations and molecular dynamics in general.

By performing the integration in Eq.(2), the van Vleck propagator is derived

$$\langle \mathbf{q}_t | e^{-i\hat{H}t/\hbar} | \mathbf{q}_0 \rangle \approx \sum_{\substack{\text{classical} \\ \text{paths}}} \sqrt{\frac{1}{(2\pi i\hbar)^F} \left| -\frac{\partial^2 S_t^{cl}(\mathbf{q}_0, \mathbf{q}_t)}{\partial \mathbf{q}_t \partial \mathbf{q}_0} \right|} e^{iS_t^{cl}(\mathbf{q}_0, \mathbf{q}_t)/\hbar - i\nu\pi/2} \quad (3)$$

$$= \sum_{\substack{\text{classical} \\ \text{paths}}} \sqrt{\frac{1}{(2\pi i\hbar)^F} \left| \frac{\partial \mathbf{q}_t}{\partial \mathbf{p}_0} \right|^{-1}} e^{iS_t^{cl}(\mathbf{q}_0, \mathbf{q}_t)/\hbar - i\nu\pi/2} \quad (4)$$

where the integral is now a sum over all classical trajectories going from \mathbf{q}_0 with initial momentum \mathbf{p}_0 to \mathbf{q}_t in an amount of time t for F degrees of freedom. ν is the Maslov or Morse index and it takes into account the number of times along each trajectory that the determinant in Eq. (3) diverges. The squared root in Eq.(3) is usually termed as the ‘‘semiclassical pre-exponential factor’’ and it embodies the second order path-fluctuations of Eq.(2). Unfortunately Eq.(3) is plagued by the improbable task of finding classical trajectories with fixed boundary values and the integrand diverges whenever the determinant is zero. The semiclassical ‘‘Initial Value Representation’’ (SC-IVR) trick introduced by Miller[4] avoids these issues by writing the wavefunction evolution in terms of the classical paths and the sum over the classical paths as a phase space integration which includes the Jacobian accounting for the change of variable

$$\langle \chi | e^{-i\hat{H}t/\hbar} | \chi \rangle \approx \int \int d\mathbf{p}_0 d\mathbf{q}_0 \sqrt{\frac{1}{(2\pi i\hbar)^F} \left| \frac{\partial \mathbf{q}_t}{\partial \mathbf{p}_0} \right|} \chi^*(\mathbf{q}_t) \chi(\mathbf{q}_0) e^{iS_t^{cl}(\mathbf{q}_0, \mathbf{p}_0)/\hbar - i\nu\pi/2} \quad (5)$$

In Eq.(5), no root search is required and the zero of the determinant at caustics is not a numerical issue anymore. The second order path-fluctuations are now represented by the square root term in Eq.(5), which quantifies how much the final position depends on the initial momentum.

A natural representation of the wavefunction in Eq.(5) is given by coherent states of the type

$$\langle \mathbf{x} | \mathbf{p}_t \mathbf{q}_t \rangle = \left(\frac{\det(\gamma)}{\pi^F} \right)^{\frac{1}{4}} e^{-\frac{1}{2}(\mathbf{x}-\mathbf{q}_t)^T \gamma (\mathbf{x}-\mathbf{q}_t) + \frac{i}{\hbar} \mathbf{p}_t^T (\mathbf{x}-\mathbf{q}_t)} \quad (6)$$

where γ is the coherent state width diagonal matrix containing time-independent coefficients. This frozen Gaussian-dressed semiclassical dynamics idea was introduced by Heller[5] and

later implemented by Herman and Kluk[6] and Kay,[7] in the case of the SC-IVR propagator of Eq.(5). The final expression for the quantum propagator is

$$\langle \chi | e^{-i\hat{H}t/\hbar} | \chi \rangle \approx \left(\frac{1}{2\pi\hbar} \right)^F \iint d\mathbf{p}_0 d\mathbf{q}_0 C_t(\mathbf{p}_0, \mathbf{q}_0) e^{\frac{i}{\hbar} S_t(\mathbf{p}_0, \mathbf{q}_0)} \langle \chi | \mathbf{p}_t \mathbf{q}_t \rangle \langle \mathbf{p}_0 \mathbf{q}_0 | \chi \rangle \quad (7)$$

where we have dropped ‘‘cl’’ for the classical action $S_t(\mathbf{p}_0, \mathbf{q}_0)$ and the original second order path-fluctuation of Eq.(2) is now equal to

$$C_t(\mathbf{p}_0, \mathbf{q}_0) = \sqrt{\det \left[\frac{1}{2} \left(\mathbf{M}_{\mathbf{q}\mathbf{q}} + \frac{1}{\gamma} \mathbf{M}_{\mathbf{p}\mathbf{p}} \gamma + \frac{i}{\hbar\gamma} \mathbf{M}_{\mathbf{p}\mathbf{q}} + \frac{\hbar}{i} \mathbf{M}_{\mathbf{q}\mathbf{p}} \gamma \right) \right]} \quad (8)$$

where $\mathbf{M}_{\mathbf{q}\mathbf{q}}$, etc., are elements of the $F \times F$ monodromy (or stability) matrix[67]

$$\mathbf{M}(t) \equiv \begin{pmatrix} \mathbf{M}_{\mathbf{p}\mathbf{p}} & \mathbf{M}_{\mathbf{p}\mathbf{q}} \\ \mathbf{M}_{\mathbf{q}\mathbf{p}} & \mathbf{M}_{\mathbf{q}\mathbf{q}} \end{pmatrix} = \begin{pmatrix} \partial \mathbf{p}_t / \partial \mathbf{p}_0 & \partial \mathbf{p}_t / \partial \mathbf{q}_0 \\ \partial \mathbf{q}_t / \partial \mathbf{p}_0 & \partial \mathbf{q}_t / \partial \mathbf{q}_0 \end{pmatrix}. \quad (9)$$

In a system following the classical Hamilton equations of motion for $(\mathbf{p}_t, \mathbf{q}_t)$, as enforced by the stationary condition of the action $S_t(\mathbf{p}_0, \mathbf{q}_0)$ of Eq.(2), the evolution of the monodromy matrix in Eq.(9) is

$$\frac{d}{dt} \mathbf{M}(t) = \begin{pmatrix} \mathbf{0} & -\mathbf{K}_t \\ \mathbf{m}^{-1} & \mathbf{0} \end{pmatrix} \mathbf{M}(t) \quad (10)$$

where $\mathbf{K}_t = \partial^2 V(\mathbf{q}_t) / \partial \mathbf{q}_t^2$ is the local Hessian, $V(\mathbf{q}_t)$ is the potential of the system, and \mathbf{m}^{-1} is the inverse of the mass tensor and it is equal to the identity in mass-scaled coordinates. The SC-IVR of Eq.(7) has been successfully employed in many fields using several variants. It provides a globally uniform asymptotic approximation to the quantum propagator. Each monodromy matrix element describes the dependency of the phase space trajectory $(\mathbf{p}_t, \mathbf{q}_t)$ with respect to its initial conditions $(\mathbf{p}_0, \mathbf{q}_0)$. Thus, the matrix \mathbf{M} is the classical representation of the quantum fluctuations about a classical trajectory.[68] Unfortunately, the semiclassical pre-exponential factor poses two main serious issues for the application of the SC-IVR propagator to complex systems. First, the calculation of $C_t(\mathbf{p}_0, \mathbf{q}_0)$ represents the bottleneck as the dimensionality of the problem increases, because the numerical effort per trajectory has an unfavorable scaling with respect to the number of degrees of freedom. Then, for chaotic dynamics, the monodromy matrix elements become exponentially large, with the exponent being the Lyapunov number, which is needed to properly account for the strong dependency on the initial conditions. This amplifies the oscillatory behavior of the phase space integrand and undermines the accuracy and feasibility

of any numerical approaches to evaluate the phase space integration necessary to obtain the semiclassical propagator.[69] The only way out rather than exponentially improving the number of trajectories to have the chaotic trajectories contribution mutually cancelled,[70] it is to find reasonable approximations for the calculation of $C_t(\mathbf{p}_0, \mathbf{q}_0)$. The goal of this paper is to provide suitable approximations to avoid the pre-exponential factor to become huge. However, such an approximation cannot simply consist in the complete neglect of the pre-exponential factor, which would generally be a very rough and so not desirable approximation. In fact, in the \hbar expansion of the Schroedinger equation solution given by Miller and Kay,[9] the semiclassical propagator (and thus the pre-exponential factor) appears at zero-th order. Furthermore, also in the perturbation approach of Pollak and co-workers, $C_t(\mathbf{p}_0, \mathbf{q}_0)$ turns out already in the unperturbated zero order term.[71]

Kay[70] has proposed to simply remove the trajectories that are unstable and that cause the trouble, whenever along the evolution

$$|C_t(\mathbf{p}_0, \mathbf{q}_0)|^2 \geq D_t \tag{11}$$

where D_t is a time dependent or independent quantity. One can choose D_t according to the target value. In our cases, the target values are the vibrational energy levels and a D_t equals to the number of trajectories does not perturb our results. In this procedure, discarded trajectories still contribute to the Monte Carlo phase space integration at times preceding the rejection. Thus, also chaotic trajectories contributes to the propagator, but at shorter times. When rejecting trajectories in the Monte Carlo integration of Eq.(7), one should ask himself if enough trajectories would survive the removal process to provide any useful semiclassical information. Miller and coworkers[72] came up with a numerical approach borrowed from quantum scattering calculations. They formulate the pre-exponential factor evolution in terms of log-derivative quantities. On one hand, this approach avoids the branch cut problem which has hampered other formulations. On the other, the numerical issues induced by the chaotic dynamics still remains. Another possible solution is the “poor person’s” approximation.[73] Here, the pre-exponential factor is taken to be constant with respect to the phase space Monte Carlo integration and approximated to the one of the most probable trajectory, according to the Husimi distribution of the integrand in Eq.(7).

Unfortunately, none of these procedures completely eliminate the problems arising from chaotic trajectories and practical schemes need to be developed in order to adopt the semi-

classical propagator for obtaining quantum information of complex systems. The present work tests previous approximations of the pre-exponential factor $C_t(\mathbf{p}_0, \mathbf{q}_0)$ and proposes new and more efficient ones, and shows advantages with regard to previous approximations.

III. SC-IVR EXPRESSION FOR POWER SPECTRUM CALCULATIONS

In this paper, the accuracy of the pre-exponential factor approximations will be tested by looking at the power spectrum $I(E)$ of several models and molecular systems. $I(E)$ is defined as

$$\begin{aligned} I(E) &\equiv \langle \chi | \delta(\hat{H} - E) | \chi \rangle \\ &= \frac{1}{2\pi\hbar} \int_{-\infty}^{+\infty} \langle \chi | e^{-i\hat{H}t/\hbar} | \chi \rangle e^{iEt/\hbar} dt \end{aligned} \quad (12)$$

where $|\chi\rangle$ is a reference state of the type $|\mathbf{p}_{eq}\mathbf{q}_{eq}\rangle$ and \hat{H} is the Hamiltonian of the system. We choose \mathbf{q}_{eq} to be the global minimum position vector with respect to the potential energy of \hat{H} and \mathbf{p}_{eq} is taken such that $p_{eq,j}^2/2m = \hbar\omega_j(n+1/2)$, where ω_j is the frequency of the j -th normal mode. The semiclassical expression of $\langle \chi | e^{-i\hat{H}t/\hbar} | \chi \rangle$ is reported in Eq.(7) and the matrix γ of (6) is taken to be diagonal and constant in time, with $\gamma_j = m\omega_j/\hbar$ for the j -th mode. The SC-IVR expression for the power spectrum calculations is obtained by substituting Eq.(7) into Eq.(12) to obtain

$$\begin{aligned} I(E) &= \frac{1}{2\pi\hbar} \int_{-\infty}^{+\infty} dt \iint d\mathbf{p}_0 d\mathbf{q}_0 e^{iEt/\hbar} \left(\frac{1}{2\pi\hbar} \right)^F \\ &\quad \times C_t(\mathbf{p}_0, \mathbf{q}_0) e^{\frac{i}{\hbar}S_t(\mathbf{p}_0, \mathbf{q}_0)} \langle \chi | \mathbf{p}_t \mathbf{q}_t \rangle \langle \mathbf{p}_0 \mathbf{q}_0 | \chi \rangle. \end{aligned} \quad (13)$$

Several approaches has been introduced to speed up the phase space integration of Eq.(13).[29, 53, 60, 74] Here we employ the time-averaging filter to reduce the number of phase space trajectories needed for the convergence of Monte Carlo integration. An additional time integration is inserted in Eq.(13), and the phase space average is performed for a time-averaged integrand. After approximating the pre-exponential factor as $C_t(\mathbf{p}_0, \mathbf{q}_0) = \exp[i\phi(t)/\hbar]$, the following time averaged semiclassical expression for the power spectrum of Eq.(13) can be obtained

$$I(E) = \left(\frac{1}{2\pi\hbar} \right)^F \iint d\mathbf{p}_0 d\mathbf{q}_0 \frac{1}{2\pi\hbar T} \left| \int_0^T dt e^{\frac{i}{\hbar}[S_t(\mathbf{p}_0, \mathbf{q}_0) + Et + \phi(t)]} \langle \chi | \mathbf{p}_t \mathbf{q}_t \rangle \right|^2. \quad (14)$$

Clearly, the longer the time-averaging T is, the greater is the advantage of the time filter.

IV. THE ADIABATIC PRE-EXPONENTIAL FACTOR APPROXIMATION

The idea of the adiabatic approximation of the pre-exponential factor $C_t(\mathbf{p}_0, \mathbf{q}_0)$ by Miller and coworkers[75, 76] is to assume that the monodromy matrix elements are adiabatic with respect to each other. The instantaneous normal mode framework is enforced by the diagonalization of the Hessian at each time-step. First, the auxiliary variables

$$\mathbf{Q}_t = \mathbf{M}_{\mathbf{q}\mathbf{q}} - i\hbar\mathbf{M}_{\mathbf{q}\mathbf{p}}\gamma \quad (15)$$

$$\mathbf{P}_t = \mathbf{M}_{\mathbf{p}\mathbf{q}} - i\hbar\mathbf{M}_{\mathbf{p}\mathbf{p}}\gamma \quad (16)$$

are introduced, and the equations of motion of \mathbf{P}_t and \mathbf{Q}_t are

$$\begin{cases} \dot{\mathbf{Q}}_t = \mathbf{P}_t \\ \dot{\mathbf{P}}_t = -\mathbf{K}_t\mathbf{Q}_t \end{cases} \quad (17)$$

where initial conditions $\mathbf{Q}_0 = \mathbf{1}$ and $\mathbf{P}_0 = -i\hbar\gamma$ can be obtained from Eqs. (9) and (10). Then, the pre-exponential factor of Eq.(8) becomes

$$C_t(\mathbf{p}_0, \mathbf{q}_0) = \sqrt{\frac{1}{2^F} \det \left[\mathbf{Q}_t + \frac{i}{\hbar\gamma} \mathbf{P}_t \right]}. \quad (18)$$

This formulation is still exact. The set of instantaneous mass-scaled normal mode coordinates is calculated at each time step by the matrix \mathbf{U}_t such that

$$\mathbf{U}_t^\dagger \mathbf{K}_t \mathbf{U}_t \equiv \omega_t^2 \quad (19)$$

where ω_t^2 is the instantaneous diagonal Hessian matrix. In the adiabatic approximation the time derivatives of \mathbf{U}_t are neglected and the new transformed matrices

$$\tilde{\mathbf{Q}}_t \equiv \mathbf{U}_t^\dagger \mathbf{Q}_t \mathbf{U}_t \quad (20)$$

$$\tilde{\mathbf{P}}_t \equiv \mathbf{U}_t^\dagger \mathbf{P}_t \mathbf{U}_t \quad (21)$$

remain diagonal at all times t . The system of equations (17) for the new variables of Eqs. (20) and (21) becomes a set of F -independent one-dimensional second-order differential equations. Finally, the expression of the pre-exponential factor in the adiabatic approximation is

$$C_t(\mathbf{p}_0, \mathbf{q}_0) \approx \sqrt{\prod_j^F \frac{1}{2} \left(\tilde{Q}_t(j, j) + \frac{i}{\hbar\gamma} \tilde{P}_t(j, j) \right)} \quad (22)$$

where $\tilde{Q}_t(j, j)$ and $\tilde{P}_t(j, j)$ are the diagonal elements of the matrices respectively defined in Eqs. (20) and (21) and evolved according to Eq.(17). This approximation should be good as far as each frequency $\omega_{j,t}$ of the $j - th$ mode is well separated and modes are not strongly coupled, i.e. adiabatic with respect to each other. The opposite situation, the diabatic limit, when frequencies are in resonance, is also favorable to the adiabatic approximation, since the instantaneous normal mode diagonalization can fit a local adiabatic representation. The intermediate cases, where coupling cannot be removed, are the worse case scenario for the adiabatic approximation.

The basic advantages of this approximation is to reduce the computational cost. However, integration of Eq.(17) is still sensitive to the initial conditions and problems related to chaotic dynamics will hinder a straightforward application of Eq.(22).

V. THE “POOR PERSON’S” APPROXIMATION

A more drastic approximation is the “poor person’s” one, that we will abbreviate as “PPs”. [73] This approximation is motivated by the observation that the approximated propagator should (i) be exact for harmonic systems, (ii) be not very sensitive to the choice of the coherent states width parameter, (iii) be local in the potential, and (iv) retains normalization. Given the conditions (i)-(iv), the approximation should also save computational time, making complex systems simulations possible. The PPs formulation approximates Eq.(7) as

$$\langle \chi | e^{-i\hat{H}t/\hbar} | \chi \rangle \approx \left(\frac{1}{2\pi\hbar} \right)^F C_t(\mathbf{p}_{eq}, \mathbf{q}_{eq}) \iint d\mathbf{p}_0 d\mathbf{q}_0 e^{\frac{i}{\hbar} S_t(\mathbf{p}_0, \mathbf{q}_0)} \langle \chi(\mathbf{p}_{eq}, \mathbf{q}_{eq}) | \mathbf{p}_t \mathbf{q}_t \rangle \langle \mathbf{p}_0 \mathbf{q}_0 | \chi(\mathbf{p}_{eq}, \mathbf{q}_{eq}) \rangle \quad (23)$$

where the phase point $(\mathbf{p}_{eq}, \mathbf{q}_{eq})$ is the location of the coherent reference state $|\chi\rangle$ and the center of the Husimi distribution employed for the Monte Carlo phase space sampling. In this way, the pre-exponential factor C_t is calculated for a single (and the most probable) trajectory and enforced to all the others. Eq.(23) is exact for the harmonic oscillator, where C_t does not depend on the phase space initial coordinates. The monodromy matrix still needs to be calculated for the trajectory starting at $(\mathbf{p}_{eq}, \mathbf{q}_{eq})$ and the approximation can not be applied when the system is so chaotic that the monodromy matrix of that single trajectory can not be evolved. The PPs approximation is particularly advantageous for “on the fly” simulations, where the Hessian calculation is very demanding.

VI. THE LOG-DERIVATIVE FORMULATION OF THE PRE-EXPONENTIAL FACTOR AND ITS APPROXIMATIONS

To overcome the numerical issues of the monodromy matrix evolution described above, Miller and coworkers wrote the evolution of the pre-exponential factor $C_t(\mathbf{p}_0, \mathbf{q}_0)$ using the log-derivative formulation.[72] The log-derivative matrix \mathbf{R}_t is defined by

$$\mathbf{R}_t = \frac{\dot{\mathbf{Q}}_t}{\mathbf{Q}_t} = \frac{\mathbf{P}_t}{\mathbf{Q}_t} \quad (24)$$

and it is properly defined since $\det(\mathbf{Q}_t)$ is never zero.[7, 70] The pre-exponential factor can now be written as

$$C_t(\mathbf{p}_0, \mathbf{q}_0) = \sqrt{\det \left[\frac{1}{2} \left(I + \frac{i}{\hbar\gamma} \mathbf{R}_t \right) \right]} e^{\frac{1}{2} \int_0^t d\tau \text{Tr}[\mathbf{R}_\tau]} \quad (25)$$

and one is left with the calculation of the matrix \mathbf{R}_t at each time step. By deriving Eq.(24) on both sides with respect to time and using Eq.(17), the equation of motion

$$\dot{\mathbf{R}}_t = -\mathbf{K}_t - \mathbf{R}_t^2 \quad (26)$$

is what must be solved for the calculation of the pre-exponential factor. No approximation has been introduced so far and Eq.(25) is an exact formulation of the pre-exponential factor. The issues related to the stability matrix for chaotic systems are hidden inside the integration of the Riccati's equation (26). A possible simplification is to assume that the force constant matrix \mathbf{K}_t is slowly varying and one can set the squared root in Eq.(25) equal to unity. However, this approximation does not remove the numerical issues related to chaotic motion. For these reasons, one should better employ the following approximations.

A. The Harmonic approximation

This is a crude approximation which is equivalent to take at any time in Eq. (26)

$$\mathbf{K}_t \approx \mathbf{K}_0 = \omega_0^2 \quad (27)$$

where ω_0^2 are the diagonal Hessian matrix elements at equilibrium position. Since, for harmonic oscillators, the coherent state width matrix γ is constant and equal to $m\omega_0/\hbar$, the solution of Eq.(26) is analytical

$$\mathbf{R}_t = -\hbar\gamma \frac{i + \tan(\hbar\gamma t)}{1 - i \tan(\hbar\gamma t)} = -i\hbar\gamma \quad (28)$$

and the pre-exponential factor is approximated as

$$C_t(\mathbf{p}_0, \mathbf{q}_0) = e^{-i\hbar \sum_{j=1}^F \gamma_j t/2} = e^{-i \sum_{j=1}^F \omega_{0,j} t/2} \quad (29)$$

where $\omega_{0,j}$ is the harmonic frequency of the j -th mode. The same result can be obtained by inserting \mathbf{K}_0 into Eq.(10) and solving the set of differential equations.

B. The Johnson Multichannel approximation

To improve the accuracy of the harmonic approximation, one can naively replace in Eq.(29) $\omega_{0,j}t$ with $\int_0^t \omega_{\tau,j} d\tau$, i.e. the initial harmonic frequencies with instantaneous ones and consider the integral over time. A more elegant way to reach the same conclusion is to assume that the term $\dot{\mathbf{R}}_t$ in Eq.(26) can be disregarded since the log-derivative matrix \mathbf{R}_t is much more slowly variant than \mathbf{Q}_t . The equation solution of Eq.(26) becomes

$$\mathbf{R}_t = -i\sqrt{\mathbf{K}_t} \quad (30)$$

where the minus sign has been chosen to satisfy the initial conditions $\mathbf{R}_0 = -i\hbar\gamma$. By inserting Eq.(30) into Eq.(25), the following approximation is obtained

$$C_t(\mathbf{p}_0, \mathbf{q}_0) = \sqrt{\det \left[\frac{1}{2} \left(\mathbf{I} + \frac{\sqrt{\mathbf{K}_t}}{\hbar\gamma} \right) \right]} e^{-i \int_0^t \text{Tr}(\sqrt{\mathbf{K}_\tau}) d\tau/2}. \quad (31)$$

The pre-exponential term in Eq.(31) is also slowly variant and by approximating each matrix element ratio

$$\frac{\omega_{t,j}}{\hbar\gamma_j} \approx 1 \quad (32)$$

the Johnson's "multichannel WKB" approximation of the semiclassical pre-exponential factor is derived

$$C_t(\mathbf{p}_0, \mathbf{q}_0) \approx \exp \left[-\frac{i}{\hbar} \int_0^t \sum_{j=1}^F \left(\frac{\hbar}{2} \omega_{\tau,j} \right) d\tau \right]. \quad (33)$$

Eq.(33) approximates the pre-exponential factor as the phase arising from the local zero-point energy along the trajectory. This approximation has already been employed in the past.[36, 77–80]

C. A recursive perturbative approach

A possible accuracy improvement of the Sec.VI A is the following perturbative approach. We initially follow Miller and coworkers,[72] and we assume that \mathbf{R}_t is given by the harmonic value in Eq.(28) corrected by a perturbation term ε

$$\mathbf{R}_t = -i\hbar\gamma + \varepsilon. \quad (34)$$

By inserting (34) into the Riccati's equation (26), and assuming the perturbation constant in time, i.e. $\dot{\varepsilon} \approx 0$,

$$-\mathbf{K}_t + \hbar^2\gamma^2 = \varepsilon^2 - 2i\hbar\gamma\varepsilon \quad (35)$$

and neglecting the higher order terms in ε , the following expression for the perturbation term is obtained

$$\varepsilon = -\frac{i}{2} \left(\frac{\mathbf{K}_t}{\hbar\gamma} - \hbar\gamma \right). \quad (36)$$

The resulting approximation of the log-derivative matrix (24) is

$$\mathbf{R}_t^{(1)} = -\frac{i}{2} \left(\hbar\gamma + \frac{\mathbf{K}_t}{\hbar\gamma} \right) \quad (37)$$

as previously suggested by Miller.[72] Eq.(37) will provide the approximate pre-exponential factor once inserted into Eq.(25). Since the Hessian \mathbf{K}_t is always real, the expression of $\mathbf{R}_t^{(1)}$ in Eq.(37) is purely imaginary. This pre-exponential factor approximation mainly differs from the harmonic (29) and Johnson's (33) ones in the exponential term, which is linearly dependent on the Hessian.

We now want to systematically improve the approximation (37). The idea is to use Eq.(37) as a more accurate solution than the harmonic one (28), insert it into the Riccati equation and obtain a new perturbative correction. A new solution will be obtained by iteratively using the new correction as an initial guess. We start by inserting

$$\mathbf{R}_t^{(2)} = \mathbf{R}_t^{(1)} + \varepsilon = -\frac{i}{2} \left[\frac{\mathbf{K}_t}{\hbar\gamma} + \hbar\gamma \right] + \varepsilon \quad (38)$$

into (26), and disregard higher order and time-derivative terms of ε and Hessian time-derivatives. We obtain the following equation

$$0 = \frac{1}{4} \left(\hbar^2\gamma^2 + \frac{\mathbf{K}_t^2}{\hbar^2\gamma^2} + 2\mathbf{K}_t \right) + i\varepsilon \left(\frac{\mathbf{K}_t}{\hbar\gamma} + \hbar\gamma \right) - \mathbf{K}_t \quad (39)$$

which brings

$$\boldsymbol{\varepsilon} = \frac{i \left(\hbar\gamma - \frac{\mathbf{K}_t}{\hbar\gamma} \right)^2}{4 \frac{\mathbf{K}_t}{\hbar\gamma} + \hbar\gamma}. \quad (40)$$

Then, the substitution of Eq.(40) into Eq.(38) provides the expression

$$\mathbf{R}_t^{(2)} = -\frac{i}{2} \left[\frac{\mathbf{K}_t}{\hbar\gamma} + \hbar\gamma \right] + \frac{i \left(\hbar\gamma - \frac{\mathbf{K}_t}{\hbar\gamma} \right)^2}{4 \left(\hbar\gamma + \frac{\mathbf{K}_t}{\hbar\gamma} \right)}. \quad (41)$$

Again, this solution is purely imaginary and the dependence on the Hessian matrix is more complex than previous ones. Eq.(41) is better written in terms of $\mathbf{R}_t^{(1)}$ as

$$\mathbf{R}_t^{(2)} = \mathbf{R}_t^{(1)} + \frac{1}{2^3} \frac{\left(\hbar\gamma - \frac{\mathbf{K}_t}{\hbar\gamma} \right)^2}{\mathbf{R}_t^{(1)}}. \quad (42)$$

We can now look for the next order $\mathbf{R}_t^{(3)} = \mathbf{R}_t^{(2)} + \boldsymbol{\varepsilon}$ by inserting this guess into the Riccati's equation, take zero time derivative for \mathbf{K}_t and $\boldsymbol{\varepsilon}$ as usual, and disregarding the higher order perturbation terms, we obtain

$$\mathbf{R}_t^{(3)} = \mathbf{R}_t^{(2)} - \frac{1}{2^7} \frac{\left(\hbar\gamma - \frac{\mathbf{K}_t}{\hbar\gamma} \right)^4}{\mathbf{R}_t^{(1)^2} \mathbf{R}_t^{(2)}} \quad (43)$$

and, in the same fashion, one can find

$$\mathbf{R}_t^{(4)} = \mathbf{R}_t^{(3)} + \frac{1}{2^{15}} \frac{\left(\hbar\gamma - \frac{\mathbf{K}_t}{\hbar\gamma} \right)^8}{\mathbf{R}_t^{(1)^4} \mathbf{R}_t^{(2)^2} \mathbf{R}_t^{(3)}}. \quad (44)$$

By induction, the final n -order correction of the harmonic log-derivative matrix is in closed form equal to

$$\mathbf{R}_t^{(n)} = \mathbf{R}_t^{(n-1)} + \frac{(-)^n}{2^{(2^n-1)}} \frac{\left(\hbar\gamma - \frac{\mathbf{K}_t}{\hbar\gamma} \right)^{2^{(n-1)}}}{\prod_{j=0}^{n-2} \left(\mathbf{R}_t^{(n-1-j)} \right)^{2^j}}. \quad (45)$$

We stress that Eq.(45) is not the formal solution of the Riccati equation (26), even if it is a closed form for an n -th order perturbation correction, because it has assumed that the Hessian is constant, i.e. $\dot{\mathbf{K}}_t \approx 0$, throughout the derivation.

VII. NUMERICAL APPROXIMATIONS

An alternative route with respect to the analytical approximations presented in the previous Sections, is to perform numerical approximations. We consider two possibilities, the

Log-derivative symplectic integrator and the monodromy matrix regularization. We employ either one of these numerical approximations as an alternative to the analytical approximations.

A. Log-derivative symplectic integration

Another approach to solve the evolution of the monodromy matrix elements in presence of chaos is to employ high order numerical algorithms. We usually employ the $4th$ order symplectic algorithm described in Appendix of Ref.[18](c), and originally due to Calvo *et al.*,[81] to solve Eq.(10). One can similarly use such an accurate algorithm to solve the Riccati equation instead. Manolopoulos and Gray[82] showed that the system of equations

$$\begin{cases} \mathbf{X}_k &= \mathbf{R}_{k-1} + b_k \mathbf{K}_k \Delta t \\ \mathbf{R}_k &= [\mathbf{I} + a_k \mathbf{X}_k \Delta t]^{-1} \mathbf{X}_k \end{cases} \quad (46)$$

does this task when suitable coefficients a_k and b_k [82] are employed (\mathbf{X} is an auxiliary variable). We implemented Eq.(46) in our calculations. The results indicate that when the trajectory is experiencing a chaotic potential, the numerical calculation of the log-derivative \mathbf{R}_t cannot be managed, similarly to the case of the monodromy matrix elements.

B. Monodromy Matrix regularization

Another route to deal with chaotic potentials is to introduce an artificial and *ad hoc* numerical method to tame the exponentially growing value of the monodromy matrix elements. A possible procedure is to monitor the monodromy elements at each time step. After the diagonalization of the monodromy matrix, the degrees of freedom mostly responsible for the chaotic behaviour can be identified by looking at their complex eigenvalues. More specifically, each element of the monodromy matrix can be written as

$$m_{ij} = u_{ik} \lambda_k u_{kj}^{-1} \quad (47)$$

where u_{ik} and u_{kj}^{-1} are the elements of the \mathbf{U} orthogonal matrix that diagonalizes the monodromy matrix and the sum over k is implied. The greater the modulus of an eigenvalue λ_s is, the more sensitive to the initial conditions and chaotic the s -degree of freedom is. Then,

a brute force regularization approach consists in setting either the most chaotic eigenvector or eigenvalue or both equal to zero in the following way

$$\tilde{\mathbf{U}}^{-1} = \begin{pmatrix} \dots & \dots & \dots \\ 0 & 0 & 0 \\ \dots & \dots & \dots \end{pmatrix}; \quad \tilde{\mathbf{U}} = \begin{pmatrix} \dots & 0 & \dots \\ \dots & 0 & \dots \\ \dots & 0 & \dots \end{pmatrix} \quad (48)$$

where the $s - th$ column and row is set to zero and a modified diagonal matrix is obtained

$$\tilde{\mathbf{\Lambda}} = \begin{pmatrix} \dots & & \\ & 0 & \\ & & \dots \end{pmatrix} \quad (49)$$

by setting to zero the $s - th$ diagonal element of the $\mathbf{\Lambda}$ eigenvalues matrix. The criterion for setting the eigenvector or the eigenvalue equal to zero is when $|\lambda_s| \geq \epsilon_{thr}$, where ϵ_{thr} is an arbitrary positive number. Considering that for unstable manifolds monodromy matrix eigenvalues are real, this criterion can be directly applied by checking the absolute value of the real eigenvalues. A tamed monodromy matrix $\tilde{\mathbf{M}}$ suitable for time evolution is then obtained by transforming back the modified eigenvalues matrix $\tilde{\mathbf{\Lambda}}$ using the modified orthogonal matrices $\tilde{\mathbf{U}}$

$$\tilde{\mathbf{M}} = \tilde{\mathbf{U}}\tilde{\mathbf{\Lambda}}\tilde{\mathbf{U}}^{-1}. \quad (50)$$

A possible procedure for applying Eq.(50) is to monitor the larger real eigenvalues and apply either Eqs. (48) or (49) or both whenever this is above ϵ_{thr} . Numerical tests showed either choice is equivalent. However, it may be necessary to apply the regularization to more than a single degree of freedom, when the system is very chaotic. We applied multiple regularizations when a single one failed to limit numerical divergence.

VIII. NUMERICAL TESTS

To assess the accuracy of the pre-exponential factor $C_t(\mathbf{p}_0, \mathbf{q}_0)$ approximations introduced above, we consider both chaotic model potentials, as well as real molecular systems. The chaotic potentials are the bidimensional Henon-Heiles potential[83] and a bidimensional quartic potential.[70, 85] These examples are famously chaotic systems and their accurate spectrum calculation represents a tough challenge for semiclassical dynamics. Spectra have

been calculated using both Eq.(13), and the time-averaged expression of Eq.(14). The second set of systems is represented by molecules of growing dimensionality and complexity, i.e. H₂, H₂O, CO₂, H₂CO, CH₄, and CH₂D₂, and the spectra has been calculated using Eq.(14). When the pre-exponential factor is not approximated, the semiclassical trajectories are rejected either if $1 - \det |\mathbf{M}^T(t) \mathbf{M}(t)| > 10^{-5}$, which is a quite strict criteria for the accuracy of the monodromy matrix $\mathbf{M}(t)$ evolution, or using Kay's ad hoc method of Eq.(11). In alternative, when using the numerical regularization of Subsection VII B, we tested different threshold values for the highest monodromy matrix eigenvalue, and we found out that $\epsilon_{thr} = 1.15 \times 10^3$ is high enough to not perturb vibrational spectra for both model and molecular systems. This set of examples will allow the reader to fully appreciate the accuracy of the approximations for future applications, not only for models but also for real molecular systems. In the following, unless specified, atomic units ($\hbar = 1$) are adopted.

A. Bidimensional Henon-Heiles potential

Our first example of a model chaotic potential is the bidimensional Henon-Heiles potential

$$V(x, y) = \frac{1}{2}(x^2 + y^2) + \lambda x^2 y - \frac{\lambda}{3} y^3 \quad (51)$$

where the mass and the harmonic frequencies are taken to be equal to unit. The λ parameter modulates the amount of chaos added to the otherwise harmonic motion. There are four stationary points for this potential. The minimum is at the origin and the others are saddle points. We choose to look at the power spectrum for two values of λ . One is $\lambda = 0.11803$, which is the same employed by others,[54, 83] and it represents a soft chaos motion. The other is $\lambda = 0.400$ and it reproduces a quite strongly chaotic motion, as far as we are aware never considered before in semiclassical dynamics. For case 1 and 2 below, the length of a typical semiclassical trajectory with an approximated pre-exponential factor is 5000 time steps of 0.1 a.u. each. Semiclassical results are compared with exact quantum mechanical Discrete Variable Representation (DVR) calculations.[84]

Case 1: Soft chaos The power spectrum is calculated employing Eq.(13) and sampling 10^7 trajectories for the Monte Carlo integration, which is already enough for convergence. The sampling is performed such that the position center is set equal to the equilibrium positions and the momentum center is located at the first harmonic vibrational level, i.e.

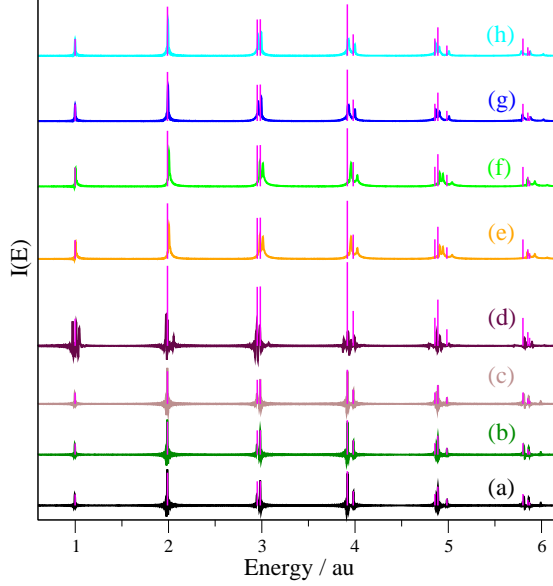


Figure 1. SC-IVR spectra of a bidimensional Henon-Heiles potential with $\lambda = 0.11803$ using Eq.(13). (a) Black continuous lines are for the rejection criterium $1 - \det |\mathbf{M}^T(t) \mathbf{M}(t)| > 10^{-5}$; (b) dark green continuous lines for the rejection method of Kay (11); (c) brown for the regularization of the monodromy matrix (50); (d) maroon for the PPs approximation; (e) orange for the harmonic pre-exponential factor approximation of Eq.(29); (f) light green spectrum for the approximation in Eq.(37) $\mathbf{R}_t^{(1)}$; (g) blue for the pre-exponential factor reported in Eq.(41) $\mathbf{R}_t^{(2)}$ and (h) cyan for Eq.(43) $\mathbf{R}_t^{(3)}$. Exact quantum mechanical values are indicated by the vertical magenta lines with an height which is equal to the square of the overlap between the SC reference state and the exact eigenstate calculated by DVR.

$p_j = \sqrt{3\hbar\omega_j}$ in mass-scaled coordinates, where ω_j is the harmonic frequency of the $j - th$ mode. This choice is evident when observing that the second and third peaks in Fig.(1) are the most intense ones. The coupling $\lambda = 0.11803$ is small and only 28% of the trajectories are rejected using $1 - \det |\mathbf{M}^T(t) \mathbf{M}(t)| > 10^{-5}$, while 26% using Kay's criterium of Eq.(11), as it should be for a soft chaotic regime. We find the two rejection criteria to be very similar in terms of accuracy, shape of the spectra and number of rejected trajectories. Instead, 10^6 trajectories are more than enough to converge the Monte Carlo integration for the calculation of the spectra using Eq.(13) in conjunction with the analytical and the numerical pre-exponential factor approximations described above. Fig.(1) reports the power spectra at the level of Eq.(13). The bottom spectra (a) is calculated using the $\det |\mathbf{M}^T(t) \mathbf{M}(t)|$

rejection criterium, while (b) using Eq.(11). The two spectra are almost identical. As far as the numerical regularization of Eq.(50) reported at spectrum (c), the results are in very good agreement with (a) and (b). Only 28% (the same percent of the determinant rejection criterium) trajectories have been regularized and the most chaotic one was tamed for 278 times out of 5000 steps. Spectrum (d) is computed with the PPs pre-exponential factor approximation of section V, while spectrum (e) refers to the harmonic pre-exponential factor of section VIA. Spectrum (f) is obtained by using $\mathbf{R}_t^{(1)}$ approximation of Eq.(37), while (g) and (h) derive from our ansatzs presented in Section VIC and formulated in Eq.(41) and Eq.(43) respectively. Fig.(1) shows quite a good agreement, both in peak position and intensity between all approximations and the SC-IVR results. The prefactor approximations formulated in Eq.(41) and Eq.(43) works better than the harmonic and $\mathbf{R}_t^{(1)}$ approximations. The Johnson approximation of sec.VIB cannot be applied for the Henon-Heiles potential because $\omega_{j,t}$ in Eq.(33) is often imaginary, making the exponential term too big to be calculated (overflowing code error). The adiabatic approximation couldn't be applied, since Eq.s (20) and (21) are too chaotic and cannot be integrated numerically. The computed energy levels are reported in Table (I).

When using the time averaged power spectrum approximation of Eq.(14), we run only 5000 trajectories after verifying that 10^3 trajectories are enough to reach numerical convergence. The results are reported in Fig. (2) at different level of approximation. The bottom spectra (a) and (b) are calculated by using Eq.(14) and without any of the pre-exponential factor approximations. Starting from the bottom, (c) is performed by using Eq.(50), where 12% of trajectories have been regularized and for the most chaotic one Eq.(50) is employed 99 times. Spectrum (d) is at the level of adiabatic approximation (see Section (IV)), the spectrum (e) is computed with the PPs pre-exponential factor approximation of section V, (f) refers to the harmonic pre-exponential factor of section VIA, the (g) spectrum is obtained by using $\mathbf{R}_t^{(1)}$ approximation of Eq.(37), (h) and (i) derive from our ansatzs presented in Section VIC and formulated in Eq.(41) and Eq.(43). We observe a quite good agreement between all approximations and the original SC-IVR calculations, both in peak position and intensity. The Johnson approximation can not be applied also in this case. In addition respect to Fig.(1), we can apply the adiabatic approximation, since less trajectories are required for the time averaged spectrum. Table (II) confirms the accuracy of the separable time-averaging SC-IVR (14) values reported in the second column with respect to the exact

Table I. Power spectrum of the Henon-Heiles potential with $\lambda = 0.11803$. Comparison between results (in Atomic Units) obtained using Eq.(13) at different level of approximation. From left to right: Exact DVR values, SC-IVR values using the rejection criterium $1 - \det |\mathbf{M}^T(t) \mathbf{M}(t)| > 10^{-5}$, SC-IVR calculation using the ad hoc Kay's rejection method of Eq.(11), SC-IVR calculation using the monodromy matrix regularization (50), the PPs approximation (23), the harmonic approximation (29), $\mathbf{R}_t^{(1)}$ approximation (37), and our approximations of Eqs. (41) and (43). In the last row the Mean Average Errors (MAE) are reported.

Exact	SC-IVR	Kay's method	Regularization	PPs	HO	$\mathbf{R}_t^{(1)}$	$\mathbf{R}_t^{(2)}$	$\mathbf{R}_t^{(3)}$
0.998	0.995	0.995	0.995	0.971	1.003	1.003	0.998	0.998
1.989	1.987	1.987	1.987	1.974	2.004	2.004	1.994	1.994
1.989	1.987	1.987	1.987	1.974	2.004	2.004	1.994	1.994
2.951	2.947	2.948	2.948	2.948	2.979	2.979	2.962	2.961
2.984	2.983	2.983	2.983	2.980	3.012	3.012	2.995	2.994
2.984	2.983	2.983	2.983	2.980	3.012	3.012	2.995	2.994
3.917	3.92	3.920	3.920	3.920	3.958	3.958	3.931	3.931
3.918	3.92	3.920	3.920	3.920	3.958	3.958	3.931	3.931
3.980	3.982	3.982	3.983	3.995	4.025	4.025	4.000	3.999
3.984	3.982	3.982	3.983	3.995	4.025	4.025	4.000	3.999
4.856	4.873	4.873	4.874	4.876	4.907	4.907	4.868	4.864
4.888	4.889	4.889	4.889	4.910	4.942	4.942	4.906	4.903
4.888	4.889	4.889	4.889	4.910	4.942	4.942	4.906	4.903
4.985	4.985	4.985	4.986	5.009	5.041	5.041	5.008	5.007
4.985	4.985	4.985	4.986	5.009	5.041	5.041	5.008	5.007
5.800	5.812	5.811	5.811	5.818	5.849	5.849	5.795	5.783
5.800	5.812	5.811	5.811	5.818	5.849	5.849	5.795	5.783
5.853	5.862	5.862	5.862	5.833	5.863	5.863	5.882	5.878
5.872	5.878	5.878	5.878	5.898	5.928	5.928	5.882	5.878
MAE	0.004	0.004	0.004	0.015	0.038	0.038	0.013	0.013

Table II. Time averaged spectra for the Henon-Heiles potential with $\lambda = 0.11803$. Comparison between results (in Atomic Units) obtained with different approximations. From left to right: Exact values, TA-SC-IVR values (14) using the rejection criterium $1 - \det |\mathbf{M}^T(t) \mathbf{M}(t)| > 10^{-5}$, TA-SC-IVR calculation using the ad hoc Kay's rejection method of Eq.(11), monodromy matrix regularization (50), adiabatic approximation (22), PPs approximation (23), harmonic approximation (29), $\mathbf{R}_t^{(1)}$ approximation (37), and our approximations of Eqs. (41) and (43). In the last row the Mean Average Errors (MAE) are reported.

Exact	SC-IVR	Kay's method	Regularization	Adiabatic	PPs	HO	$\mathbf{R}_t^{(1)}$	$\mathbf{R}_t^{(2)}$	$\mathbf{R}_t^{(3)}$
0.998	0.995	0.995	0.995	0.998	0.965	1.003	1.003	0.997	0.997
1.989	1.988	1.988	1.988	1.995	1.967	2.004	2.004	1.993	1.993
1.989	1.988	1.988	1.988	2.012	2.001	2.038	2.038	2.007	2.005
2.951	2.901	2.901	2.901	2.923	2.913	2.950	2.950	2.917	2.917
2.984	2.983	2.983	2.982	3.004	2.994	3.031	3.031	2.997	2.996
2.984	2.983	2.983	2.982	3.004	2.994	3.031	3.031	2.997	2.996
3.917	3.893	3.893	3.893	3.916	3.907	3.943	3.942	3.911	3.910
3.918	3.893	3.893	3.893	3.916	3.907	3.943	3.942	3.911	3.910
3.980	3.975	3.975	3.975	3.997	3.987	4.024	4.023	3.993	3.992
3.984	3.975	3.975	3.975	3.997	3.987	4.024	4.023	3.993	3.992
4.856	4.805	4.805	4.805	4.828	4.818	4.854	4.853	4.822	4.821
4.888	4.886	4.886	4.886	4.909	4.899	4.935	4.934	4.902	4.912
4.888	4.886	4.886	4.886	4.909	4.899	4.935	4.934	4.902	4.912
4.985	4.970	4.97	4.97	4.99	4.968	5.005	5.004	4.984	4.984
4.985	4.970	4.97	4.97	5.003	4.968	5.005	5.004	5.002	5.000
5.800	5.798	5.798	5.798	5.820	5.810	5.846	5.845	5.811	5.812
5.800	5.798	5.798	5.798	5.820	5.810	5.846	5.845	5.811	5.812
5.853	5.859	5.859	5.859	5.835	5.857	5.894	5.893	5.874	5.870
5.872	5.879	5.879	5.879	5.902	5.892	5.929	5.927	5.896	5.894
MAE	0.011	0.011	0.012	0.017	0.016	0.033	0.032	0.014	0.015

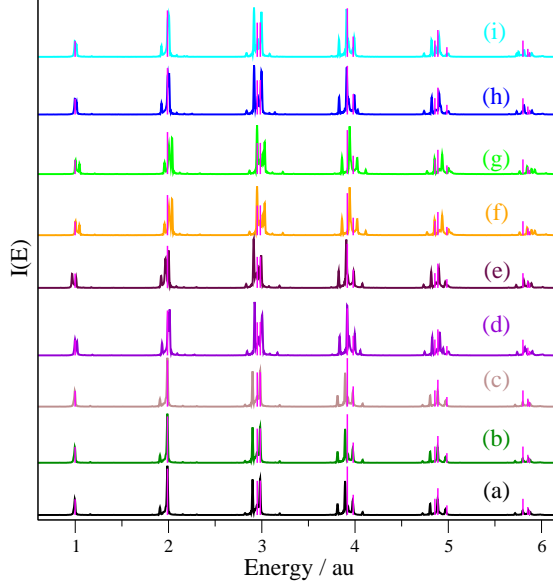


Figure 2. TA-SC-IVR (Eq.(14)) spectra of a bidimensional Henon-Heiles potential with $\lambda = 0.11803$. (a) Black continuous lines are for semiclassical spectra (14) using the rejection criterium $1 - \det |\mathbf{M}^T(t) \mathbf{M}(t)| > 10^{-5}$; (b) dark green continuous lines are for the rejection method of Kay (11); (c) brown for the regularization of the monodromy matrix (50); (d) violet for the adiabatic approximation in Eq.(22); (e) maroon for the PPs approximation; (f) orange for the harmonic pre-exponential factor approximation (Eq.(29)); (g) light green spectrum for the approximation in Eq.(37) $\mathbf{R}_t^{(1)}$; (h) blue for the pre-exponential factor reported in Eq.(41) $\mathbf{R}_t^{(2)}$ and (i) cyan for the pre-exponential factor reported in Eq.(43) $\mathbf{R}_t^{(3)}$. Exact quantum mechanical values are indicated by the vertical magenta lines with an height which is equal to square of the overlap between the SC reference state $|\chi\rangle$ and the exact eigenstate calculated by DVR.

ones in the first column, calculated by DVR. For the soft chaos Henon-Heiles power spectrum calculation, SC-IVR displays an energy mean average error (MAE) which is about 1% of the zero point value. The “Regularization” column shows that the artificial numerical regularization of Eq.(50) is not influential again, showing the negligible contribution of the chaotic trajectories to the spectrum calculation of this system. In this case the prefactor approximations have been tested on the top of the separable approximation. All other columns report the results with different pre-exponential factor approximations and they should be compared with the SC-IVR ones. $\mathbf{R}_t^{(1)}$ approximation (37), and the harmonic oscillator one (29) are, as before, quite similar and they usually overestimate the exact and semiclassical

results as expected, since they do not properly account for anharmonicity. Also the PPs overestimates by about the same amount. The adiabatic approximation (22) in the fourth column is more accurate than the PPs, the Harmonic and $\mathbf{R}_t^{(1)}$ ones, but still overestimates the original SC-IVR values. Finally, the ansatzs of Eq.(41) and (43), are the better performing pre-exponential factor analytical approximations and quite similar to the adiabatic one, where no harmonic assumptions have been introduced.

Case 2: Strong chaos

We now look at a strong chaotic motion scenario by increasing the value of the coupling term to $\lambda = 0.4$. For this value of λ , states above the ground one are quasi-bound and complex valued. Nevertheless, the SC-IVR can reproduce the real part of the vibrational eigenvalues. In the case of Eq.(13), due to the high rejection ratio, we sample 10^8 trajectories in conjunction with the $\det |\mathbf{M}^T(t) \mathbf{M}(t)|$ and Kay's criterium, while 10^7 trajectories are more than enough for the prefactor approximated spectra calculation. The system is so chaotic, that Eq.(50) could not avoid the monodromy matrix elements numerical divergence to infinity when applied either to the modulus of the biggest real eigenvalue or to the moduli of the real eigenvalues greater than ϵ_{thr} . The PPs approximation lead to a spectrum which is too noisy to find peaks, and for this reason we choose to do not report it in Fig. (3). Each peak value is reported in Table (III).

Again the two rejection criteria seem to lead to very similar spectra. The present approximations show comparable results and better than the Harmonic and $\mathbf{R}_t^{(1)}$ ones. The spectra are reported in Fig.(3). In the case of TA-SC-IVR calculations we sampled 50000 trajectories for the Monte Carlo integration of Eq.(14) rejecting 91% of the trajectories when using both rejection criteria. Instead, 5000 trajectories are enough for the approximated pre-exponential factor calculations. All power spectra are reported in Fig. (4) and each peak value is reported in Table (IV).

The original semiclassical values reported in the second column are less accurate in this case. Nevertheless, the MAE is still about 3% the zero point energy value. As in the Herman-Kluk calculation of Eq.(13), it is not possible to obtain the spectrum with the monodromy matrix regularization. Once again, the harmonic and $\mathbf{R}_t^{(1)}$ approximations are quite similar. The PPs approximation is on average overestimating the peak values. As

Table III. Henon-Heiles potential with $\lambda = 0.4$. Column labels as in Table (I).

Ex.	SC-IVR	Kay's method	HO	$\mathbf{R}_t^{(1)}$	$\mathbf{R}_t^{(2)}$	$\mathbf{R}_t^{(3)}$
0.986	0.918	0.918	1.003	1.003	0.953	0.967
1.081	1.078	1.073	1.106	1.092	1.011	1.01
1.084	1.078	1.073	1.106	1.092	1.011	1.01
1.092	1.078	1.073	1.106	1.016	1.011	1.01
1.883	1.886	1.886	2.018	2.018	1.902	1.932
1.884	1.886	1.886	2.018	2.018	1.902	1.945
2.437	2.368	2.367	2.714	2.713	2.517	2.508
2.706	2.693	2.694	2.779	2.779	2.653	2.647
2.708	2.693	2.694	2.779	2.779	2.653	2.647
MAE	0.022	0.023	0.085	0.089	0.054	0.061

Table IV. Henon-Heiles potential with $\lambda = 0.4$. Column labels as in Table (II).

Ex.	TA-SC-IVR	Kay's method	Adiabatic PPs	HO	$\mathbf{R}_t^{(1)}$	$\mathbf{R}_t^{(2)}$	$\mathbf{R}_t^{(3)}$
0.986	0.949	0.949	0.98	0.889	1.004	1.003	0.945 0.973
1.081	1.078	1.077	1.088	1.093	1.102	1.003	1.083 1.083
1.084	1.078	1.077	1.088	1.093	1.102	1.023	1.083 1.083
1.092	1.078	1.077	1.088	1.093	1.102	1.023	1.102 1.097
1.883	1.895	1.895	1.789	1.900	2.015	2.015	1.900 1.881
1.884	1.895	1.895	1.942	1.900	2.015	2.015	1.900 1.881
2.437	2.373	2.373	2.436	2.402	2.517	2.516	2.544 2.312
2.706	2.761	2.761	2.591	2.722	2.722	2.676	2.687
2.708	2.761	2.761	2.659	2.722	2.722	2.676	2.687
MAE	0.028	0.029	0.038	0.027	0.049	0.044	0.028 0.021

stressed above, the pre-exponential factor approximated results should be compared with the SC-IVR column and the better MAE of the last PPs approximation is probably due to compensation of errors. Finally, the strong chaotic regime confirms the better level of accuracy of the perturbative recursive approximations of Eqs. (41) and (43).

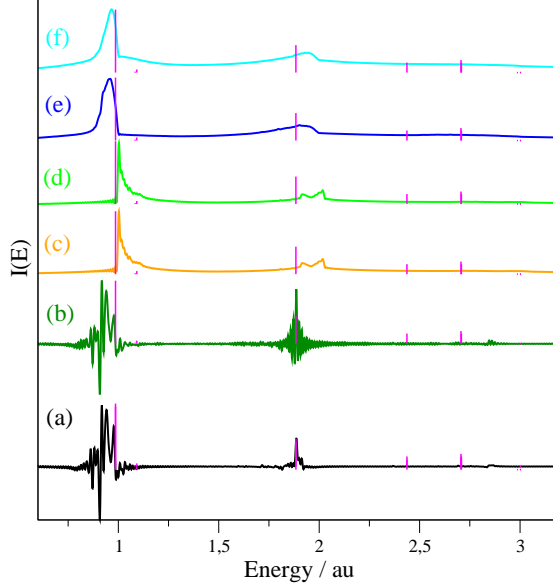


Figure 3. SC-IVR spectra of a bidimensional Henon-Heiles potential with $\lambda = 0.4$ using Eq.(13). (a) Black continuous lines are for the rejection criterium $1 - \det |\mathbf{M}^T(t) \mathbf{M}(t)| > 10^{-5}$; (b) dark green continuous lines for the rejection method of Kay (11); (c) orange for the harmonic pre-exponential factor approximation (Eq.(29)); (d) light green spectrum for $\mathbf{R}_t^{(1)}$ approximation in Eq.(37); (e) blue for the pre-exponential factor reported in Eq.(41) and (f) cyan for the pre-exponential factor reported in Eq.(43). Exact quantum mechanical values are indicated by the vertical magenta lines with an height which is equal to square of the overlap between the SC reference state and the exact eigenstate calculated by DVR.

B. Bidimensional quartic-like potential

We now consider an even more severe chaotic model, the bidimensional potential of two Morse oscillators with a significant quartic potential contribution of the type

$$V(\mathbf{q}) = \sum_{i=1}^2 D \left[1 - e^{-\alpha_i(q_i - q_i^{eq})} \right]^2 + \lambda \left[\frac{\beta}{4} \left((q_1 - q_1^{eq})^4 + (q_2 - q_2^{eq})^4 \right) + (q_1 - q_1^{eq})^2 (q_2 - q_2^{eq})^2 \right] \quad (52)$$

where $\mathbf{q} \equiv (q_1^{eq}, q_2^{eq})$ is the equilibrium position, D and α_i are the one-dimensional unitary mass Morse parameters, β tunes the amount of quartic oscillator contributions and λ also the amount of coupling between the oscillators. The Morse potential parameters are such that the equilibrium position is at the origin, $D = 0.2$ a.u., the frequencies $\omega_1 = 3000 \text{ cm}^{-1}$ and $\omega_2 = 1700 \text{ cm}^{-1}$. The parameters of the quartic potential are $\beta = 0.02$ a.u. and λ is

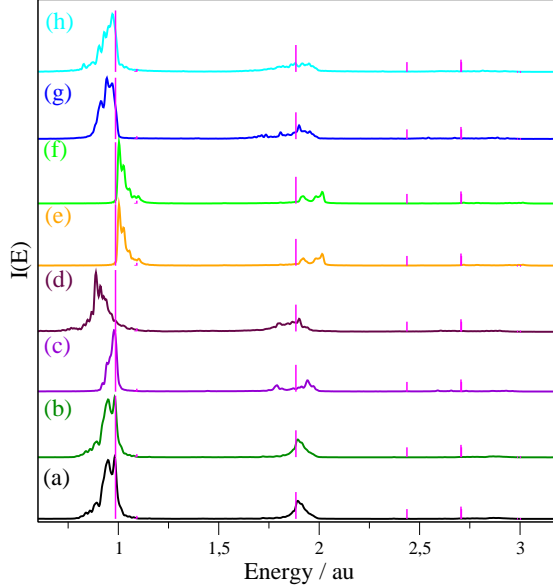


Figure 4. TA-SC-IVR spectra of a bidimensional Henon-Heiles potential with $\lambda = 0.4$. a) Black continuous lines are for semiclassical spectra (14) using the rejection criterium $1 - \det |\mathbf{M}^T(t) \mathbf{M}(t)| > 10^{-5}$; (b) dark green continuous lines are for semiclassical spectra computed using the rejection method of Kay; (c) violet for the adiabatic approximation in Eq.(22); (d) maroon for the PPs approximation; (e) orange for the harmonic pre-exponential factor approximation (Eq.(29)); (f) light green spectrum for $\mathbf{R}_t^{(1)}$ approximation in Eq.(37); (g) blue for the pre-exponential factor reported in Eq.(41) and (h) cyan for the pre-exponential factor reported in Eq.(43). Exact quantum mechanical values are indicated by the vertical magenta lines with an height which is equal to square of the overlap between the SC reference state and the exact eigenstate calculated by DVR.

tuned according to the amount of chaos one wants to introduce. If we would had taken a pure quartic oscillator which has been studied in past years,[70, 85] on one side, we would have not had any Hessian term in the potential and the previous approximation could have not been tested. On the other side, this would not be realistic since *ab initio* calculations of equilibrium properties of real molecule is such that Hessian and normal modes can be calculated. As in the case of the Henon-Heiles potential, we consider two values of coupling λ , which correspond to small and strong coupling.

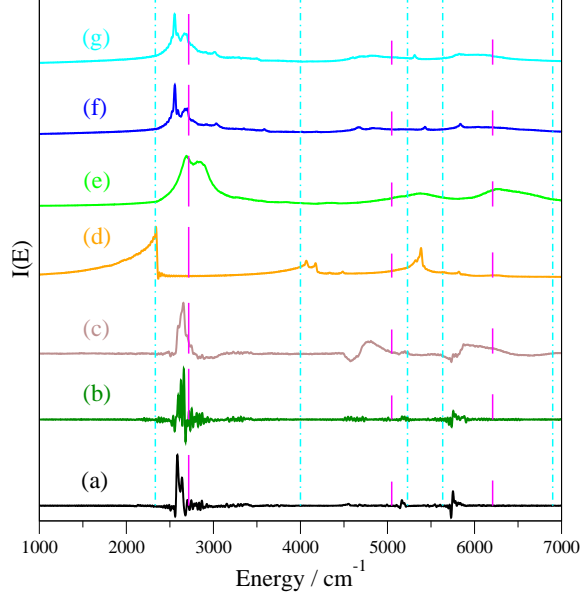


Figure 5. Power spectrum of the potential (52) with $\lambda = 10^{-6}$ using Eq.(13) and its approximations. (a) Black line for the rejection criterium $1 - \det |\mathbf{M}^T(t) \mathbf{M}(t)| > 10^{-3}$, (b) dark green line for Kay's rejection method of Eq. (11), (c) brown line for the spectrum computed using the regularization procedure (50), (d) orange line for the HO spectrum, (e) light green line for the $\mathbf{R}_t^{(1)}$ approximation spectrum, (f) blue line for the spectrum computed using Eq.(41), and (g) cyan line for the spectrum computed using Eq.(43). The vertical magenta lines represent the exact energy levels with an intensity equals to square of the overlap between the SC reference state and the exact eigenstate calculated by DVR. The vertical cyan dash-dotted lines represents the uncoupled Morse potential energy levels.

Case 1: $\lambda = 1 \cdot 10^{-6}$

We run 10^8 trajectories to overcome the high rejection rate, which is 97% for the $1 - \det |\mathbf{M}^T(t) \mathbf{M}(t)| > 10^{-3}$ criterium and 96% using Eq. (11). Instead, for the approximated prefactor approximations, 10^7 classical trajectories are enough since there is no rejection in this case. Each trajectory is 5000 time-steps long, and each time-step is 10 a.u. long. The Herman-Kluk spectra of Eq.(13) reproduce approximately the first three energy levels as shown in Figure (5). From the same Figure, the two rejection criteria lead to very similar spectra and the regularization procedure provides features quite similar to the original Herman-Kluk spectrum, in particular for the ZPE peak. The Johnson, the adiabatic and

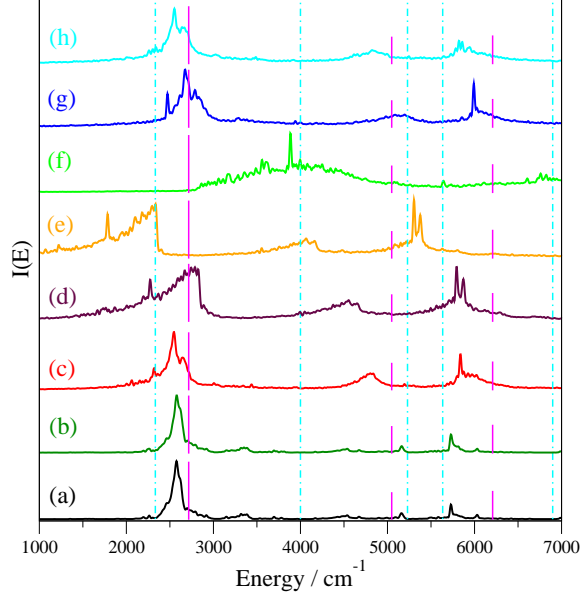


Figure 6. Power spectrum of the potential (52) with $\lambda = 10^{-6}$ using the time averaged formula of Eq.(14). (a) Black line for the rejection criterium $1 - \det |\mathbf{M}^T(t) \mathbf{M}(t)| > 10^{-3}$, (b) dark green line for the Kay's rejection method of Eq. (11), (c) red line for the Johnson's approximation spectrum, (d) maroon line for the spectrum computed using the PPs approximation, (e) orange line for the HO spectrum, (f) light green line for the $\mathbf{R}_t^{(1)}$ approximation spectrum, (g) blue line for the spectrum computed using Eq.(41), and (h) cyan line for the spectrum computed using Eq.(43). The vertical magenta lines represent the exact energy levels with an intensity equals to the square of the overlap between the SC reference state $|\chi\rangle$ and the exact eigenstate calculated by DVR. The vertical cyan dash-dotted lines are the uncoupled Morse potential energy levels.

the PPs approximations of Secs. (VIB), (IV), and (V) respectively, lead to too noisy spectra for energy levels to be detected. The harmonic approximation results are very similar to the uncoupled energy levels, while approximation of Eq.(37) and our proposed ones of Eqs. (43) and (41) give quite good results.

When calculating the spectra using the TA-SC-IVR expression of Eq.(14), we run 80000 trajectories when the rejection criteria are used, and 5000 trajectories when we use the approximations of the pre-exponential factor propagators. The numerical taming of Eq.(50) can not avoid the numerical issues when the cut-off is applied both to the modulus of the biggest real eigenvalue and to the moduli of the real eigenvalues greater than ϵ_{thr} .

Fig.(6) reports the power spectra at different semiclassical pre-exponential factor level

of approximation using Eq.(14). The (a) spectrum is the original TA-SC-IVR spectrum of Eq.(14) using $1 - \det |\mathbf{M}^T(t) \mathbf{M}(t)| > 10^{-3}$, while the spectrum (b) is obtained employing the ad-hoc method of Kay (11). The (c) spectrum is obtained using the Johnson’s approximation (33), the (d) spectrum is computed using the PPs approximation (23), the (e) spectrum the harmonic approximation (29), the (f) spectrum using $\mathbf{R}_t^{(1)}$ approximation (37), the (g) spectrum using $\mathbf{R}_t^{(2)}$, and, finally, the (h) spectrum using $\mathbf{R}_t^{(3)}$. The exact values are indicated as vertical magenta lines with intensity equals to the overlap between the SC reference state $|\chi\rangle$ and the DVR eigenvector, while the uncoupled Morse oscillators values are the vertical dot-dashed cyan lines. The adiabatic approximation couldn’t be applied, since Eq.s (20) and (21) are too chaotic and cannot be integrated numerically.

The TA-SC-IVR is quite approximated in this case and it approximately reproduces the first three peaks. It presents a ghost peak at about 3400 cm^{-1} and the highest peak is significantly shifted toward the uncoupled Morse value. Johnson’s approximation is mimicking quite well the sequence of exact peaks, while the PPs is mainly reproducing the ground energy peak. The $\mathbf{R}_t^{(1)}$ approximation spectrum is too noisy to judge. The harmonic approximation is definitely shifted toward the uncoupled Morse oscillators values, while the present approximations of Eqs. (41) and (43) are well reproducing the exact values. In particular, the higher order correction of Eq.(43) is more accurate with respect to the (a) TA-SC-IVR spectrum. This extreme example tells us that when the system is strongly chaotic, the semiclassical separable time-averaging SC-IVR is not very accurate and the approximated pre-exponential factors can better mimic the exact spectroscopic sequence.

Case 2: $\lambda = 2.5 \cdot 10^{-6}$

Since we want to test the pre-exponential factor approximations to even more extreme (and probably unrealistic) cases, we consider an even bigger coupling value between the Morse and the quartic part of the potential. We run the same number of trajectories of the previous case for the Herman-Kluk expression of Eq.(13). With these values of λ , the regularization method fails because of the highly chaotic regime of the potential. This is proved by the high ratio of rejected trajectories, 99.1% and 98.6% found when the alternative rejection criteria $1 - \det |\mathbf{M}^T(t) \mathbf{M}(t)| > 10^{-3}$ and Eq. (11) are employed. Again, the two spectra are quite similar, while the harmonic approximation is more similar to the

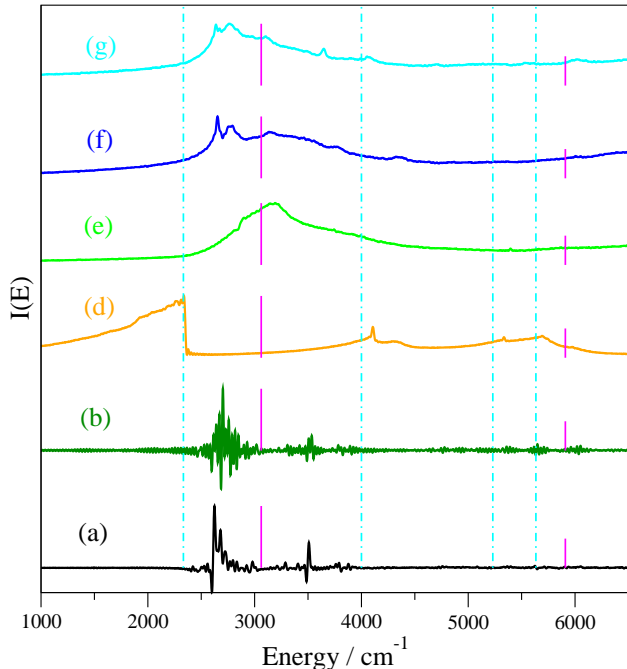


Figure 7. The same as in Fig.(5) but with λ equals to $2.5 \cdot 10^{-6}$.

uncoupled eigenvalues than the coupled ones. The $\mathbf{R}_t^{(1)}$ approximation seems to work very well, while the approximations of Eqs. (41) and (43), follow the original SC-IVR spectrum. When TA-SC-IVR calculations are employed, we run 250000 trajectories for 5000 time-steps of 10 a.u. each, of which 98.3% are rejected using $1 - \det |\mathbf{M}^T(t) \mathbf{M}(t)| > 10^{-3}$ and 97.5% using the method of Kay of Eq. (11). The approximated pre-exponential factor calculations are performed as above, i.e. with 5000 trajectories. The monodromy matrix regularization fails as in the previous case. Instead, the Johnson approximation lead to a resolute spectrum. The harmonic approximation is reproducing peaks in harmonic sequence and the $\mathbf{R}_t^{(1)}$ approximation is too noisy. The only reasonable results are those by Johnson and the new approximations of Eqs. (41) and (43). In more details, the TA-SC-IVR zero point energy (ZPE) is 2620 cm^{-1} , 2746 cm^{-1} for the Johnson approximation, 2885 cm^{-1} for Eq.(41) and 2688 cm^{-1} for the higher order approximation of Eq.(43). Once again, Eq.(43) is more similar to the original TA-SC-IVR values. However, at any semiclassical level of calculation, the first fundamental is reproduced.

Overall, the present approximation of Eq.(43) is the most accurate in these model potential energy surface scenarios. We now turn into real molecules potential energy surfaces.

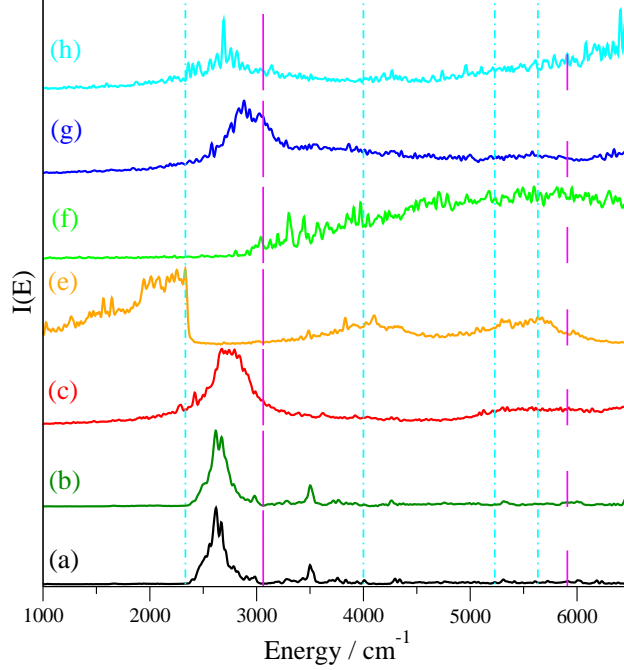


Figure 8. The same as in Fig.(6) but with λ equals to $2.5 \cdot 10^{-6}$.

C. H₂O molecule

The water molecule presents strong intermode couplings. In the calculations presented here, we employ the PES provided by Bowman[86] and Eq.(14). Each trajectory is 1000 time-step long with the single time step 10 a.u. long for a total of 8000 trajectories both with exact and approximated pre-exponential factor formulations. Previous calculations[29, 60] showed that phase space Monte Carlo convergence is reached already with 4000 trajectories. To better identify each peak, we employ combinations of antisymmetric coherent states and break down each spectrum in partial spectra for each irreducible representation of the C_{2v} point group symmetry, as explained in previous publications.[31, 60] The spectra with different pre-exponential factor approximations are reported in Fig.(9). For each approximation, the A_1 and B_2 irreducible representation spectra are reported in Fig.(9) with the same color. This figure points out the major limitations of the harmonic approximation, in particular for the highest vibrational states. More specifically, the vibrational level of each state is reported in Table (V). For each vibrational state labeled in the first column, one can read the exact quantum mechanical results in the second column, the separable SC-IVR ones on the third and fourth and the approximated ones in the following columns, as labeled in the tables

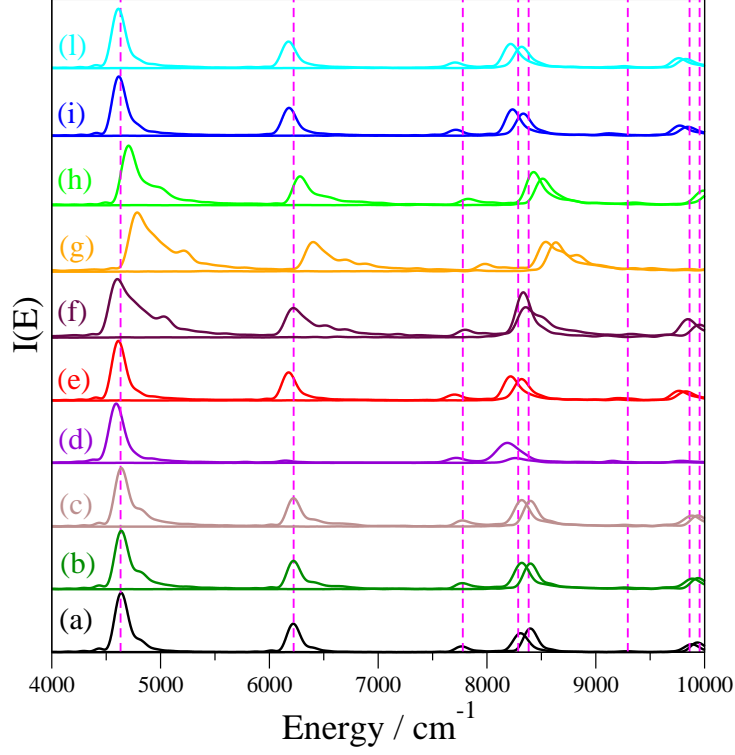


Figure 9. H₂O spectra. (a) Black line for the separable SC-IVR (14) spectrum using the rejection criterium $1 - \det |\mathbf{M}^T(t) \mathbf{M}(t)| > 10^{-5}$, (b) using the ad hoc Kay's rejection method of Eq.(11), (c) brown for the regularization of the monodromy matrix of Eq.(50), (d) violet line for the adiabatic approximation (22) spectrum, (e) red line for the Johnson's approximation (33) spectrum, (f) maroon line for the PPs approximation (23) spectrum, (g) orange line for the HO (29) approximation spectrum, (h) green line for the $\mathbf{R}_t^{(1)}$ approximation (37) spectrum, (i) blue line for the spectrum computed using $\mathbf{R}_t^{(2)}$ in Eq.(41), and (l) cyan line for the spectrum computed using $\mathbf{R}_t^{(3)}$ in Eq.(43). The vertical magenta dashed lines represent the quantum energy levels. A_1 and B_2 spectra with the same color for each approximation.

above. From the MAE, it is clear that the numerical regularization approach of Eq.(50) is very good with respect to the exact values, showing that the spectroscopic contribution of the chaotic trajectories is negligible. In fact, the monodromy matrix is regularized just for 2.1% of the total trajectories, and Eq.(50) is applied no more than 5 times per trajectory. Instead, 56% of trajectories are rejected in the standard SC-IVR calculations because of the $\det[M^T M]$ deviation from unity. This percent difference proves that most of those chaotic trajectories, that are rejected by the strict criterium $1 - \det |\mathbf{M}^T(t) \mathbf{M}(t)| > 10^{-5}$, actually

Table V. Vibrational energy levels of H₂O. Wavenumbers unit. First column reports the spectroscopic terms, second column reports the exact quantum mechanical values, third column reports the results computed with SC-IVR of Eq.(14) using the rejection criterium $1 - \det |\mathbf{M}^T(t) \mathbf{M}(t)| > 10^{-5}$, fourth column SC-IVR calculation using the ad hoc Kay’s rejection method of Eq.(11), and the others with the different pre-exponential factor approximations named as above. In the last row is reported the Mean Average Error (MAE) of each column.

State	Exact[86]	SC-IVR	Kay’s method	Regularization	Adiabatic	Johnson	PPs	HO	$\mathbf{R}_t^{(1)}$	$\mathbf{R}_t^{(2)}$	$\mathbf{R}_t^{(3)}$
ZPE	4631.6	4636	4640	4639	4592	4612	4604	4784	4704	4616	4612
$A_1(1_1)$	6222.8	6220	6220	6222	6148	6176	6220	6404	6280	6180	6176
$A_1(1_2)$	7777.7	7768	7772	7772	7716	7704	7800	7980	7828	7714	7708
$A_1(2_1)$	8287	8308	8320	8320	8188	8216	8356	8540	8428	8236	8218
$B_2(3_1)$	8382.7	8400	8400	8400	8400	8320	8334	8632	8512	8322	8319
$A_1(1_3)$	9294.1	9286	9268	9266	9156	9208	9327	9510	9352	9123	9264
$A_1(1_1 2_1)$	9862.1	9884	9888	9884	9808	9764	9952	10136	9988	9773	9764
$B_2(1_1 3_1)$	9954	9936	9940	9940	9936	9828	9846	10208	10056	9848	9827
$A_1(1_2 2_1)$	11400.5	11400	11408	11409	11280	11278	11609	11792	11508	11294	11267
$B_2(1_2 3_1)$	11490.4	11440	11440	11447	11440	11304	11342	11780	11548	11337	11305
$A_1(2_2)$	11833.9	11876	11868	11868	11660	11700	11996	12176	12004	11729	11704
$B_2(2_1 3_1)$	11886	11918	11906	11906	11920	11756	11780	12272	12076	11781	11760
$A_1(3_2)$	12069.8	12060	12044	12044	12164	11912	12224	12408	12220	11933	11900
$A_1(1_1 2_2)$	13399.1	13404	13412	13412	13294	13212	13207	13760	13536	13224	13208
$B_2(1_1 2_1 3_1)$	13443.7	13452	13440	13442	13452	13244	13276	13824	13576	13278	13254
$A_1(1_1 3_2)$	13622	13560	13560	13555		13596	13582		13712		13674
MAE		19.6	21.8	20.1	72.6	108.0	98.8	285.8	110.7	105.0	106.3

do not compromise the accuracy of the calculation. Moreover, the spectrum obtained using the rejection criterium proposed by Kay is very similar with the TA-SC-IVR one. From the following columns, it is evident that the harmonic approximation is the worse one and that $\mathbf{R}_t^{(1)}$, Johnson’s, the PPs and the new approximations $\mathbf{R}_t^{(2)}$ and $\mathbf{R}_t^{(3)}$ show about the same accuracy. Once again, the adiabatic approximation is relatively accurate when Eqs. (17)

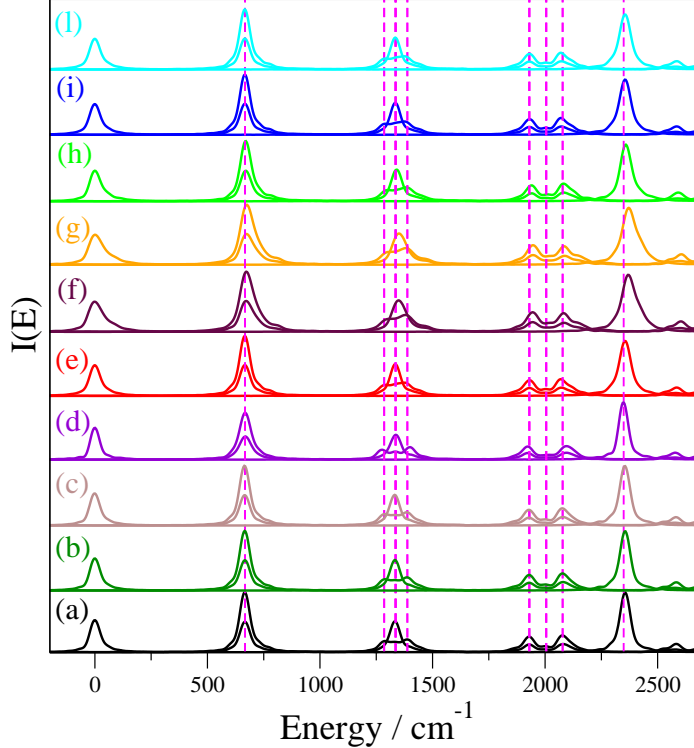


Figure 10. The same as in Fig.(9) but for the CO_2 molecule. Each approximation includes the spectra of the A_g , B_{1u} , B_{2u} and B_{3u} irreducible representations of the D_{2h} point group symmetry.[30] can be calculated.

D. CO_2 molecule

To test the accuracy of the approximations in the case of strong Fermi resonances, we choose as a test case the carbon dioxide molecule.[30, 87] We employ Chedin’s potential[88] and compare with the exact quantum mechanical results by Vasquez *et al.*[87] Each trajectory is 3000 time-steps long with a time-step 10 a.u. long. We employ 15000 trajectories for the phase space integration both with and without the pre-exponential factor approximations, which is by far enough for Monte Carlo convergence. Fig.(10) shows a good agreement between all approximations. Carbon dioxide has higher molecular weight than water and its dynamics is probably more classical. Table(VI) reports the values of each vibrational level for each approximation. In this case, all approximations are quite accurate, as noted above. The harmonic oscillator approximation is again the less accurate one, followed by the PPs and $\mathbf{R}_t^{(1)}$ ones. Surprisingly, also the adiabatic is not very accurate. The present approxima-

Table VI. The same as in Table (V) but for CO₂.

State	Exact[87]	SC-IVR	Kay's method	Regularization	Adiabatic	Johnson	PPs	HO	$\mathbf{R}_t^{(1)}$	$\mathbf{R}_t^{(2)}$	$\mathbf{R}_t^{(3)}$
<i>ZPE</i>	2536.15	2535	2535	2536	2531	2534	2539	2564	2541	2534	2534
(000)	667.47	667	667	665	669	666	673	672	670	666	666
(01 ¹ 0)	667.47	667	667	666	669	666	673	672	670	666	666
(01 ¹ 0)	1285.1	1290	1288	1288	1275	1290	1299	1297	1294	1286	1291
(10 ⁰ 0)	1335.95	1333	1332	1332	1335	1334	1350	1351	1341	1334	1334
(02 ² 0)	1335.95	1333	1332	1334	1335	1334	1350	1351	1341	1334	1334
(02 ² 0)	1387.93	1388	1384	1386	1400	1383	1382	1393	1391	1382	1374
(02 ² 0)	1929.56	1930	1928	1928	1923	1933	1947	1940	1940	1931	1931
(11 ¹ 0)	1929.56	1930	1928	1929	1923	1933	1947	1940	1940	1931	1931
(11 ¹ 0)	2005.25	1997	2001	2001	2015	2003	2021	2021	2012	2003	2003
(03 ³ 0)	2005.25	1997	2001	2001	2015	2003	2021	2021	2012	2003	2003
(03 ³ 0)	2078.15	2081	2080	2077	2093	2070	2083	2086	2084	2071	2071
(03 ¹ 0)	2078.15	2081	2080	2079	2093	2070	2083	2084	2084	2071	2071
(03 ¹ 1)	2349.38	2356	2355	2354	2347	2356	2371	2373	2359	2356	2354
MAE		3.0	2.7	2.1	6.9	3.8	11.4	12.4	6.3	3.2	3.9

tions ($\mathbf{R}_t^{(2)}$ and $\mathbf{R}_t^{(3)}$) and Johnson's one are the most accurate and with almost no difference with respect to the original SC-IVR integration. The disappointing performance of the adiabatic approximation is probably due to the coupling of the CO₂ modes, which is intermediate between the fully adiabatic and diabatic regime. The numerical taming approach of Eq.(50) is as accurate as the reference SC-IVR calculation. Their similarity is explained by the small (0.6%) percentage of trajectory correction using Eq.(50) with respect to the 14% rejected by looking at the determinant of the monodromy matrix and 8% evaluating $|C_t(\mathbf{p}_0, \mathbf{q}_0)|^2$. The numerical taming is employed no more than 4 times per trajectory.

E. CH₂O molecule

Passing from 3 to 4 atom molecules, we choose to test the pre-exponential factor approximations with the formaldehyde vibrational spectrum, since this is a well tested case.

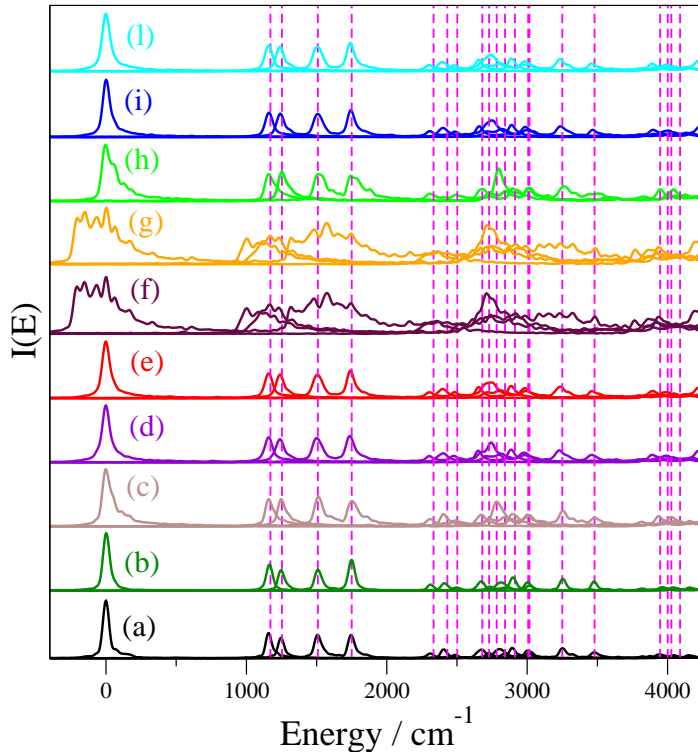


Figure 11. The same as in Fig.(9) but for the CH_2O molecule. Each approximation includes the spectra of the A_1 , A_2 , B_1 and B_2 irreducible representations of the C_{2v} point group symmetry.

Also, CH_2O presents light atoms, as well as strongly coupled dynamics. We employ the PES designed by Martin *et al.*[89] and we compare our semiclassical results with the exact quantum mechanical calculations by Carter *et al.*[90] We employ 24000 trajectories for the SC-IVR calculations without pre-exponential factor approximation (except for the basic one implied by the separable approximation) and we reject 82.5% with the monodromy matrix determinant criterion and 85.6% by using Eq. (11). Instead, 8000 trajectories are used for the approximated and numerically tamed pre-exponential factor. All trajectories are evolved for 3000 time-steps with a time-step 10 a.u. long for all simulations. The point group symmetry is C_{2v} , and spectra for all four irreducible representations are reported at each approximation level of accuracy in Fig.(11).

The CH_2O spectrum can be divided into a low energy region, populated by the fundamentals of four vibrational modes, and an higher energy region, where one can find the fundamentals of the remaining modes and several overtones. Since the accuracy of each approximation looks similar in Fig.(11), we report in Tables (VII) and (VIII) each vibrational state value.

Table VII. The same as in Table (V) but for the fundamentals of CH₂O.

simmetry	Ex.[90]	SC-IVR	Kay's method	Regularization	Adiabatic	Johnson	PPs	HO	$\mathbf{R}_t^{(1)}$	$\mathbf{R}_t^{(2)}$	$\mathbf{R}_t^{(3)}$
ZPE (A_1)		5774	5774	5780	5744	5744	5932	6112	5819	5744	5744
B_1 (1_1)	1171	1162	1162	1169	1160	1159	1000	1004	1159	1160	1158
B_2 (2_1)	1253	1245	1246	1248	1240	1240	1164	1168	1253	1240	1240
A_1 (3_1)	1509	1509	1506	1513	1501	1509	1573	1575	1516	1509	1506
A_1 (4_1)	1750	1747	1745	1752	1737	1743	1745	1743	1745	1745	1740
A_1 (5_1)	2783	2810	2810	2785	2745	2747	2708	2711	2799	2750	2741
B_2 (6_1)	2842	2850	2846	2836		2801	2862	2741	2846	2807	2800

Table VIII. The same as in Table (V) but for the overtones of CH₂O.

State	Exact[90]	SC-IVR	Kay's method	Regularization	Adiabatic	Johnson	PPs	HO	$\mathbf{R}_t^{(1)}$	$\mathbf{R}_t^{(2)}$	$\mathbf{R}_t^{(3)}$
A_1 (1_2)	2333	2310	2310	2309	2302	2308	2163	2453	2307	2307	2304
A_2 ($1_1 2_1$)	2431	2410	2408	2405	2403	2399	2356	2360	2408	2401	2396
A_1 (2_2)	2502	2497	2494	2489	2477	2486		2712	2495	2486	2480
B_1 ($1_1 3_1$)	2680	2672	2670	2675	2654	2656	2736		2679	2658	2654
B_2 ($2_1 3_1$)	2729	2731	2730	2728	2800	2719	2762	2761	2734	2723	2716
B_1 ($1_1 4_1$)	2913	2898	2896	2896	2886	2887	2871		2896	2888	2889
B_2 ($2_1 4_1$)	3007	3002	3002	3002	2976	2986	2946		3010	2989	2983
A_1 (3_2)	3016	3018	3014	3018	2986	2996	3086		3022	2993	3010
A_1 ($3_1 4_1$)	3250	3254	3252	3256	3230	3240	3157		3263	3238	3234
A_1 (4_2)	3480	3476	3475	3480	3462	3463	3323		3516	3468	3460
B_1 ($1_1 5_1$)	3947	3957	3960	3937	3892	3897	3864	3868	3949	3897	3890
A_2 ($1_1 6_1$)	4001	3979	3978	3974	3941	3942	3858	3864	3977	3945	3944
B_2 ($2_1 5_1$)	4027	4056	4054	4029	3990	3994	3934	3938	4045	4010	3994
A_1 ($2_1 6_1$)	4089	4038	4034	4043	4042	4053	4196		4074	4048	4048
A_1 ($3_1 5_1$)	4266	4275	4273	4268	4218	4225	4481	4216	4281	4225	4216
MAE		12.8	13.1	9.9	31.9	25.2	91.1	91.9	12.1	23.4	30.2

For sake of comparison, Table (VII) shows only the fundamentals excitations and Table (VIII) the overtones. The MAE reported in the last row of Table (VIII) is calculated over results reported in both tables. For this molecule, the harmonic approximation is so drastic, that most of the peaks are missing. As far as the other approximations are concerned, the PPs is similar to the harmonic one, the adiabatic approximation is a little bit more accurate, followed by the Johnson one. $\mathbf{R}_t^{(2)}$ of Eq.(41) and $\mathbf{R}_t^{(3)}$ of Eq.(43) are quite accurate. In this case also $\mathbf{R}_t^{(1)}$ is very accurate. As far as the numerical regularization is concerned, the results are very good with respect to the exact values and the ordinary SC-IVR calculation. A fraction of 20.8% of trajectories has been tamed and each one no more than 11 times. This percent proves once again that most of the chaotic trajectories rejected by the determinant criterion do not jeopardize the accuracy of the spectrum.

F. CH_4 and CH_2D_2 molecule

In terms of chaotic motion, methane and dideuterated methane are quite challenging given the nine strongly coupled degrees of freedom and the light atoms dynamics. We employ the PES by Lee et al.[91] and compare with the exact quantum energy levels,[92] as done in previous semiclassical calculations.[60, (b)] We employ 32000 trajectories for the SC-IVR calculation, out of which 88.8% and 88.7% are rejected using the monodromy matrix criterium, while 98.9% and 97.4% using the criterium of Kay, respectively for the CH_4 and CH_2D_2 molecule. Instead, 14000 classical trajectories are used for the approximated and numerical tamed pre-exponential factor calculations. All trajectories are made of 3000 time-steps each, with the same time-step length as above and for all simulations. In the case of methane, the point group symmetry is T_d . The spectrum of each irreducible representation is reported in Fig.(12) with the same color code as above and for different approximations. Table (IX) shows the low lying energy levels. These can be compared to the exact ones reported, as before, in the second column. The fifth column reports the regularization results, where 37.6% of the trajectories experienced a monodromy matrix regularization for no more than 21 times. This was enough to not reject any trajectory and reproduced the quantum mechanical results quite accurately. The PPs approximation is very similar to the harmonic one. Overall, $\mathbf{R}_t^{(2)}$ and $\mathbf{R}_t^{(3)}$ are offering the most accurate pre-exponential factor approximation, a part from the adiabatic and the regularization ones that imply the

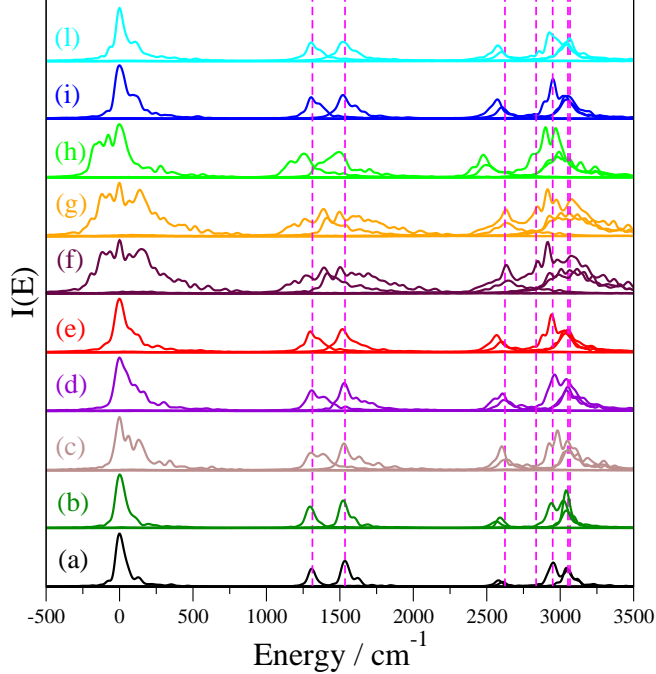


Figure 12. The same as in Fig.(9) but for the CH_4 molecule. Each approximation includes the spectra of the A_1 , E , and T_2 irreducible representations of the T_d point group of symmetry.

integration of the equation of motion of the monodromy matrix elements.

The point group symmetry for CH_2D_2 is C_{2v} and each irreducible representation is reported in Fig.(13). As in previous figures, Fig.(13) reports the results for each approximation. From this figure, results are quite similar, except for the highest vibrational levels. A more detailed view is provided by Table (X), where 44.1% of the 14000 trajectories have been regularized for no more than 19 times each. The PPs is confirming to be about as accurate as the harmonic one, and the adiabatic approximation is a quite accurate one. The Jonhson approximation is also quite accurate. The $\mathbf{R}_t^{(3)}$ approximation of Eq.(43) is overall more accurate than $\mathbf{R}_t^{(2)}$ and $\mathbf{R}_t^{(1)}$. An harmonic approximation of the pre-exponential factor would be too brutal in this case and some of the peak signals are missing.

IX. CONCLUSIONS

The series of calculations reported above show the importance of the semiclassical pre-exponential factor of Eq.(8) to properly account for the quantum mechanical effects of the semiclassical propagator. Unfortunately, the semiclassical calculation of the pre-exponential

Table IX. The same as in Table (V) but for CH₄.

State	Exact[92]	SC-IVR	Kay's method	Regularization	Adiabatic	Johnson	PPs	HO	$\mathbf{R}_t^{(1)}$	$\mathbf{R}_t^{(2)}$	$\mathbf{R}_t^{(3)}$
ZPE (A_1)	9707	9708	9708	9704	9669	9657	9846	10124	9941	9659	9652
T_2 (1_1)	1313	1296	1297	1304	1309	1300	1390	1390	1257	1305	1304
E (2_1)	1535	1524	1524	1528	1531	1518	1500	1497	1496	1522	1520
T_2 (1_2)	2624	2596	2593	2636	2616	2601	2646	2636	2497	2605	2600
T_2 ($1_1 2_1$)	2836	2820	2821	2832	1309	2818	2890	2887	2753	2827	2824
T_1 ($1_1 2_1$)	2836	2820	2821	2832	1309	2818	2890	2887	2753	2827	2824
A (3_1)	2949	2942	2942	2982	2963	2944	2914	2916	2936	2951	2928
E (2_2)	3067	3040	3042	3062	3052	3028	3065	3066	2993	3035	3044
T_2 (4_1)	3053	3038	3040	3052	3044	3037	3092	3069	2983	3041	3044
MAE		15.3	16.6	8.7	7.8	18.6	39.8	34.9	68.1	13.0	15.6

factor of classical trajectories for chaotic systems is hampered by numerical issues, as already known and once more demonstrated here on several model systems. To bypass this numerical *empasse*, we recall and present possible approximations to the pre-exponential factor in SC-IVR dynamics. These approximations are motivated either by analytical considerations or by numerical regularizations. Each approximation is presented, derived and then applied separately to both model systems with an artificial amount of chaos and real systems of growing dimensionality and complexity. The accuracy of each approximation has been tested with the Herman-Kluk and the time-averaging SC-IVR methods versus the number of rejected trajectories, which is an empirical measure of the amount of chaos as well as respect to the established ad-hoc method of Kay.[70] The numerical regularization is quite accurate but it can not be applied *a priori* for any system since it implies the calculation of the monodromy matrix. The regularization results are very similar to the original SC-IVR ones, since the chaotic trajectories are not counting in the regularized monodromy matrix. The pre-exponential factor analytical approximations, which are $\mathbf{R}_t^{(2)}$ in Eq.(41) and $\mathbf{R}_t^{(3)}$ in Eq.(43), are quite accurate compared to both the exact values and the SC-IVR ones, and we suggest them for semiclassical simulations of systems when the integration of the monodromy matrix and its regularization are not possible.

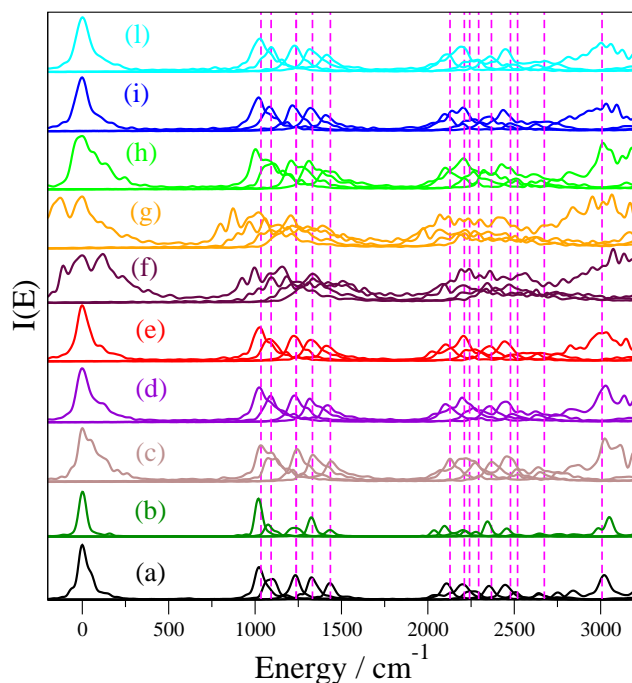


Figure 13. The same as in Fig.(9) but for the CH_2D_2 molecule. Each approximation includes the spectra of the A_1 , A_2 , B_1 and B_2 irreducible representations of the C_{2v} point group of symmetry.

ACKNOWLEDGMENTS

We acknowledge support from the European Research Council (ERC) under the European Union's Horizon 2020 research and innovation programme (grant agreement No [647107] – SEMICOMPLEX – ERC-2014-CoG). M.C. acknowledges also the CINECA and the Regione Lombardia award under the LISA initiative (grant SURGREEN) for the availability of high performance computing resources. Dr. Riccardo Conte and Prof. Dmitry Shalashilin are warmly thanked for useful discussions.

-
- [1] W. H. Miller, *Adv. Chem. Phys.* **25**, 69 (1974).
 - [2] W. H. Miller, *Proc. Natl. Acad. Sci. U.S.A.* **102**, 6660 (2005).
 - [3] K. G. Kay, *Annu. Rev. Phys. Chem.*, 2005, **56**, 255.
 - [4] W. H. Miller, *J. Chem. Phys.* **53**, 3578 (1970); W. H. Miller and T. F. George, *J. Chem. Phys.* **56**, 5668 (1972).
 - [5] E. J. Heller, *J. Chem. Phys.* **62**, 1544 (1975); E. J. Heller, *J. Chem. Phys.* **75**, 2923 (1981).

Table X. The same as in Table (V) but for CH₂D₂.

symmetry	Ex.[92]	SC-IVR	Kay's method	Regularization	Adiabatic	Johnson	PPs	HO	$\mathbf{R}_t^{(2)}$	$\mathbf{R}_t^{(2)}$	$\mathbf{R}_t^{(3)}$
ZPE (A_1)	8443	8442	8438	8440	8410	8401	8510	8860	8508	8408	8404
A_1 (1_1)	1034	1019	1018	1035	1026	1027	997	875	1003	1021	1025
B_2 (2_1)	1093	1078	1074	1076	1092	1084	1185	1056	1108	1086	1092
B_1 (3_1)	1238	1240	1224	1244	1228	1225	1335	1208	1208	1216	1228
A_2 (4_1)	1332	1326	1324	1334	1316	1323	1425	1306	1312	1321	1315
A_1 (5_1)	1436	1431	1431	1432	1421	1414			1409	1409	1413
B_2 ($1_1 2_1$)	2128	2098	2094	2128	2104	2105	2098	2068	2103	2101	2111
A_1 (6_1)	2211	2203	2202	2220	2200	2207	2194		2207	2205	2192
B_1 ($1_1 2_1$)	2242	2222	2214				2224	2344	2217	2218	2212
B_1 (7_1)	2294	2270	2276	2273	2267	2273			2265	2269	2288
A_2 ($1_1 4_1$)	2368	2349	2342	2370	2359	2360	2474	2273	2325	2358	2360
A_1 ($1_1 5_1$)	2474	2465	2455	2457	2459	2444	2359	2413	2428	2437	2448
B_2 ($2_1 5_1$)	2519	2510	2518	2512	2491	2497	2592	2456	2513	2477	2494
B_1 ($3_1 5_1$)	2674	2658	2647	2650	2631	2635	2742	2624	2656	2627	2631
A_2 ($4_1 5_1$)	2769	2764	2762	2754	2741	2745			2748	2743	2748
A_1 (8_1)	3008	3044	3048	3024	3032	3033	3074	3065	3014	3035	3000
MAE		14.6	18.1	9.7	18.5	18.3	74.7	60.3	22.9	23.4	17.5

- [6] M. F. Herman, J. Chem. Phys. **85**, 2069 (1986); E. Kluk, M. F. Herman and H. L. Davis, J. Chem. Phys. **84**, 326 (1986).
- [7] K. G. Kay, J. Chem. Phys. **100**, 4377 (1994); K. G. Kay, J. Chem. Phys. **100**, 4432 (1994).
- [8] W. H. Miller, J. Chem. Phys. **125**, 132305 (2006).
- [9] W. H. Miller, J. Chem. Phys. **125**, 132305 (2006); K. G. Kay, Chem. Phys. **322**, 3 (2006).
- [10] T. Sklarz and K. G. Kay, J. Chem. Phys. **120**, 2606 (2004).
- [11] C. Harabati and K. G. Kay, J. Chem. Phys. **127**, 084104 (2007).
- [12] G. Hochman and K. G. Kay, J. Chem. Phys. **130**, 061104 (2009).
- [13] M. F. Herman, Annu. Rev. Phys. Chem. **45**, 83 (1994).
- [14] N. Makri, Annu. Rev. Phys. Chem. **50**, 167 (1999).

- [15] (a) S. Zhang and E. Pollak, *J. Chem. Phys.* **121**, 3384 (2004); (b) S. Zhang and E. Pollak, *J. Chem. Theory Comput.* **1**, 345 (2005).
- [16] J. Shao and E. Pollak, *J. Chem. Phys.* **125**, 133502 (2006).
- [17] (a) E. Pollak and E. Martin-Fierro, *J. Chem. Phys.* **126**, 164107 (2007); (b) E. Martin-Fierro and E. Pollak, *J. Chem. Phys.* **125**, 164104 (2006).
- [18] (a) A. R. Walton, D. E. Manolopoulos, *Mol. Phys.* **87**, 961 (1996); (b) A. R. Walton, D. E. Manolopoulos, *Chem. Phys. Lett.* **244**, 448 (1995); (c) M. L. Brewer, J. S. Hulme, D. E. Manolopoulos, *J. Chem. Phys.* **106**, 4832 (1997).
- [19] S. Bonella, D. Montemayor, and D. F. Coker, *Proc. Natl. Am. Soc.* **102**, 6715 (2005).
- [20] S. Bonella and D. F. Coker, *J. Chem. Phys.* **118**, 4370 (2003).
- [21] (a) C. Harabati, J. M. Rost, and F. Grossmann, *J. Chem. Phys.* **120**, 26 (2004); (b) F. Grossmann, *Comments At. Mol. Phys.* **34**, 243 (1999).
- [22] T. F. Viscondi and M. A. M. de Aguiar, *J. Chem. Phys.* **134**, 234105 (2011).
- [23] B. B. Issack and P. N. Roy, *J. Chem. Phys.* **127**, 054105 (2007).
- [24] C. Venkataraman, *J. Chem. Phys.* **135**, 204503 (2001).
- [25] H. Nakamura, S. Nanbu, Y. Teranishic, and A. Ohtab, *Phys. Chem. Chem. Phys.* **18**, 11972 (2016)
- [26] Al. D. Kondorskiy and S. Nanbu, *J. Chem. Phys.* **143**, 114103 (2015)
- [27] M. Buchholz, F. Grossmann, and M. Ceotto, *J. Chem. Phys.* **144**, 094102 (2016)
- [28] S. Ray, P. Ostmann, L. Simon, F. Grossmann, and W.T. Strunz, *J. Phys. A: Math. Theor.* **49**, 165303 (2016)
- [29] M. Ceotto, S. Atahan, G. F. Tantardini, and A. Aspuru-Guzik, *J. Chem. Phys.* **130**, 234113, (2009).
- [30] M. Ceotto, S. Atahan, S. Shim, G. F. Tantardini, and A. Aspuru-Guzik, *Phys. Chem. Chem. Phys.* **11**, 3861 (2009).
- [31] M. Ceotto, G. F. Tantardini, and A. Aspuru-Guzik, *J. Chem. Phys.* **135**, 214108 (2011).
- [32] M. Ceotto, Y. Zhuang, and W. L. Hase, *J. Chem. Phys.* **138**, 054116 (2013).
- [33] R. Conte, A. Aspuru-Guzik, and M. Ceotto, *J. Phys. Chem. Lett.* **4**, 3407 (2013).
- [34] J. Tatchen and E. Pollak, *J. Chem. Phys.*, 2009, **130**, 041103.
- [35] R. Ianculescu, J. Tatchen, and E. Pollak, *J. Chem. Phys.* **139**, 154311 (2013).

- [36] S. Y. Y. Wong, D. M. Benoit, M. Lewerenz, A. Brown, and P.-N. Roy, *J. Chem. Phys.* **134**, 094110 (2011).
- [37] W. Chen, W. L. Hase, H. B. Schlegel, *Chem. Phys. Lett.* **228**, 436 (1994).
- [38] J. M. Millam, V. Bakken, W. Chen, W. L. Hase, H. B. Schlegel, *J. Chem. Phys.* **111**, 3800 (1999).
- [39] L. Sun and W. L. Hase, *Rev. Comput. Chem.* **19**, 79 (2003).
- [40] T. Zimmermann, J. Ruppen, B. Li, and J. Vaníček, *Int. J. Quantum Chem.* **110**, 2426 (2010).
- [41] M. Ben-Nun, T. J. Martinez, *Adv. Chem. Phys.* **121**, 439 (2002); B. G. Levine, J. D. Coe, A. M. Virshup, and Todd J. Martinez, *Chem. Phys.* **347**, 3 (2008); J. D. Coe, B. G. Levine, and T. J. Martinez *J. Phys. Chem.* **111**, 11302 (2007).
- [42] R. M. Wentzcovitch and J. L. Martins, *Solid State Commun.* **78**, 831 (1991).
- [43] D. Marx and J. Hutter, *Modern Methods and Algorithms of Quantum Chemistry*, edited by J. Grotendorst (John von Neumann Institute for Computing, Julich, Germany, 2000), 2nd ed.
- [44] L. Sun, K. Song, and W. L. Hase, *Science* **296**, 875 (2002).
- [45] H. Wang, X. Sun, and W. H. Miller, *J. Chem. Phys.* **108**, 9726 (1998).
- [46] W. H. Miller, *Faraday Disc. Chem. Soc.* **110**, 1 (1998).
- [47] W. H. Miller, *J. Phys. Chem. A* **103**, 9384 (1999).
- [48] (a) J. Liu and W. H. Miller, *J. Chem. Phys.* **125**, 224104 (2006); (b) *ibidem* **126**, 234110 (2007); (c) *ibidem* **127**, 114506 (2007); (d) *ibidem* **128**, 144511 (2008).
- [49] (a) I. Navrotskaya and E. Geva, *J. Phys. Chem. A* **111**, 460 (2007); (b) B. K. Ka, Q. Shi, and E. Geva, *J. Phys. Chem. A* **109**, 5527 (2005); (c) F. X. Vazquez, S. Talapatra, and E. Geva, *J. Phys. Chem. A* **115**, 9775 (2011).
- [50] S. Koda, *J. Chem. Phys.* **143**, 244110 (2015)
- [51] S. Koda, *J. Chem. Phys.* **144**, 154108 (2016)
- [52] J. Petersen and E. Pollak, *J. Chem. Phys.* **143**, 224114 (2015)
- [53] (a) X. Sun and W. H. Miller, *J. Chem. Phys.* **110**, 6635 (1999); (b) H. Wang, M. Thoss, K. Sorge, R. Gelabert, X. Gimenez and W. H. Miller, *J. Chem. Phys.* **114**, 2562 (2001); (c) R. Gelabert, X. Gimenez, M. Thoss, H. Wang and W. H. Miller, *J. Chem. Phys.* **114**, 2572 (2001); (d) M. Thoss, H. Wang and W. H. Miller, *J. Chem. Phys.* **114**, 9220 (2001);
- [54] H. Wang, D. E. Manolopoulos and W. H. Miller, *J. Chem. Phys.* **115**, 6317 (2001).

- [55] (a) K. Thompson and N. Makri, *Phys. Rev. E* **59**, R4729 (1999); (b) J. Shao and N. Makri, *J. Phys. Chem. A* **103**, 7753, 9479 (1999).
- [56] R. Conte and E. Pollak *Phys. Rev. E* **81**, 036704 (2010).
- [57] R. Conte and E. Pollak *J. Chem. Phys.* **136**, 094101 (2012).
- [58] (a) H. Ushiyama and K. Takatsuka, *J. Chem. Phys.* **122**, 224112 (2005); (b) S. Takahashi and K. Takatsuka, *J. Chem. Phys.* **127**, 084112 (2007)
- [59] (a) V. S. Filinov, *Nucl. Phys. B* **271**, 717 (1986); (b) N. Makri and W. H. Miller, *Chem. Phys. Lett.* **139**, 10 (1987); (c) J. D. Doll, D. L. Freeman, and T. L. Beck, *Adv. Chem. Phys.* **78**, 61 (1994); (d) S. M. Anderson, D. Neuhauser, and R. Baer, *J. Chem. Phys.* **118**, 9103 (2003).
- [60] A. L. Kaledin and W. H. Miller, *J. Chem. Phys.* **118**, 7174 (2003); A. L. Kaledin and W. H. Miller, *J. Chem. Phys.* **119**, 3078 (2003).
- [61] Y. Zhuang, M. R. Siebert, W. L. Hase, K. G. Kay, and M. Ceotto, *J. Chem. Theory and Comput* **9**, 54 (2013).
- [62] D. Tamascelli, F. S. Dambrosio, R. Conte, and M. Ceotto, *J. Chem. Phys.* **140**, 174109 (2014).
- [63] M. Ceotto, D. dell'Angelo, and G. F. Tantardini, *J. Chem. Phys.* **133**, 054701 (2010).
- [64] M. Ceotto, S. Valleau, G. F. Tantardini, and A. Aspuru-Guzik, *J. Chem Phys.* **134**, 234103 (2011).
- [65] R.P. Feynman and A.R. Hibbs, *Quantum Mechanics and Path Integrals* (McGraw-Hill Companies, 1965).
- [66] M. V. Berry and K. E. Mount, Semiclassical approximations in wave mechanics, *Rep. Prog. Phys.* **35**, 315 (1972).
- [67] H. Goldstein, *Classical Mechanics*, 2nd ed. Addison-Wesley, New York, 1988
- [68] M. Thoss and H. Wang, *Annu. Rev. Phys. Chem.*, 2004, **55**, 299.
- [69] D. Thirumalai, B.J. Berne, *Annu. Rev. Phys. Chem.* **37**, 401 (1986) ;C.H. Mak, D. Chandler, *Phys. Rev. A* **41**, 5709 (1990); J.D. Doll, D.L. Freeman, T.L. Beck, *Adv. Chem. Phys.* **78**, 61 (1994); C.H. Mak, R. Egger, H. Weber-Gottschick, *Phys. Rev. Lett.* **81**, 4533 (1998).
- [70] K.G. Kay, *J. Chem. Phys.* **101**, 2250, 1994.
- [71] J. Ankerhold, M. Saltzer, E. Pollak, *J. Chem. Phys.* **116**, 5925 (2002); E. Pollak, J. Shao, *J. Phys. Chem. A* **107**, 7112 (2003); S. Zhang, E. Pollak, *J. Chem. Phys.* **119**, 11058 (2003); S. Zhang, E. Pollak, *Phys. Rev. Lett.* **91**, 190201 (2003); S. Zhang, E. Pollak, *Phys. Rev. Lett.* **93**, 140401 (2004).

- [72] R. Gelabert, X. Gimenez, M. Thoss, H. Wang and W. H. Miller, *J. Phys. Chem. A* **104**, 10321-10327 (2000).
- [73] J. Tatchen, E. Pollak, G. Tao, and W. H. Miller, *J. Chem. Phys.* **134**, 134104 (2011).
- [74] H. Wang, D. E. Manolopoulos, and W. H. Miller, *J. Chem. Phys.* **115**, 6317 (2001).
- [75] V. Guallar, V. S. Batista and W. H. Miller, *J. Chem. Phys.* **110**, 9922 (1999).
- [76] V. Guallar, V. S. Batista and W. H. Miller, *J. Chem. Phys.* **113**, 9510 (2000).
- [77] B. B. Issack and P.N. Roy, *J. Chem. Phys.* **123**, 084103 (2005) .
- [78] B. B. Issack and P.-N. Roy, *J. Chem. Phys.* **127**, 144306 (2007).
- [79] B. B. Issack and P.-N. Roy, *J. Chem. Phys.* **126**, 024111 (2007).
- [80] B. B. Issack and P.-N. Roy, *J. Chem. Phys.* **127**, 054105 (2007)
- [81] M. P. Calvo and J. M. Sanz-Serna, *SIAM J. Sci. Comput.* **14**, 936 (1993)
- [82] D. E. Manolopoulos and S. K. Gray, *J. Chem. Phys.* **102**, 9214 (1995)
- [83] M.L. Brewer, *J. Chem. Phys.* **111**, 6168 (1999).
- [84] D. Colbert and W. H. Miller, *J. Chem. Phys.* **96**, 1982 (1992).
- [85] B. Eckhardt, G. Hose, E. Pollak, *Phys. Rev A* **39**, 3776 (1989).
- [86] J.M. Bowman, A. Wierzbicki, J. Zuniga, *Chem. Phys. Lett.* **150**, 269 (1988).
- [87] J. Vazquez, M.E. Harding, J.F. Stanton, and J. Gauss, *J. Chem. Theory Comput.* **7**, 1428 (2011).
- [88] A. Chedin, *J. Mol. Spectrosc.* **76**, 430 (1979).
- [89] J.M.L. Martin, T.J. Lee, and P.R. Taylor, *J. Mol. Spectrosc.* **160**, 105 (1993).
- [90] S. Carter, N. Pinnavaia, and N.C. Handy, *Chem. Phys. Lett.* **240**, 400 (1995).
- [91] T.J. Lee, J.M.L. Martin, P.R. Taylor, An accurate ab initio quartic force field and vibrational frequencies for CH₄ and isotopomers, *J. Chem. Phys.* **102**, 254 (1995).
- [92] S. Carter S., H.M. Shnider, J.M. Bowman, *J. Chem. Phys.* **110**, 8417 (1999).